Evaluation of a new model of aeolian transport in the presence of vegetation

Junran Li[1, 2], Gregory S. Okin[2, *], Jeffrey E. Herrick[1], Jayne Belnap[3], Mark E. Miller[4], Kimberly Vest[5], Amy E. Draut[6]

1, 2. Junran Li, USDA-ARS Jornada Experimental Range, New Mexico State University, Las Cruces, NM 88003-8003; Department of Geography, University of California-Los Angeles, CA 90095;

***Corresponding author:** okin@ucla.edu, Tel: 310-825-3426, Fax: 310-206-5976

1. Jeffrey E. Herrick, USDA-ARS Jornada Experimental Range, Las Cruces, NM 88003-8003, jherrick@nmsu.edu, Tel: 575-646-5194, 575-646-5889

2. Gregory S. Okin, Department of Geography, University of California-Los Angeles, CA 90095, okin@ucla.edu, Tel: 310-825-3426, Fax: 310-206-5976

3. Jayne Belnap, U.S. Geological Survey, Southwest Biological Science Center, Moab, UT 84532, jayne_belnap@usgs.gov, Tel: 434-719-2333, Fax: 435-719-2350

4. 4. Mark E. Miller, National Park Service, Canyonlands National Park, Moab, UT 84532, mark_e_miller@nps.gov, Tel: 435-719-2130, Fax: 435-719-2300

5. Kimberly Vest, University of Maryland Center for Environmental Sciences, Appalachian Lab, Frostburg, MD 21532, kvest@al.umces.edu, Tel: 310-689-7124, Fax: 310-689-7200

6. Amy E. Draut, U.S. Geological Survey, Pacific Science Center, Santa Cruz, CA 95060, adraut@usgs.gov, Tel: 831-427-4733, Fax: 831-427-4748

Abstract

Aeolian transport is an important characteristic of many arid and semiarid regions worldwide that is related to dust emission and ecosystem processes. The purpose of this paper is to evaluate a recent model of aeolian transport in the presence of vegetation [*Okin*, 2008]. This approach differs from previous models by modeling how vegetation affects the distribution of shear velocity on the surface rather than merely calculating the average effect of vegetation on surface shear velocity or simply using empirical relationships. Vegetation, soil, and meteorological data at 65 field sites with measurements of horizontal flux were collected from the Western US.

Measured fluxes were tested against modeled values to evaluate model performance, to obtain a set of optimum model parameters, and to estimate the uncertainty in these parameters. The same field data were used to model horizontal flux using three other schemes. Our results show that the *Okin* [2008] model can predict horizontal flux with approximate relative error of 2.1 and that further empirical corrections can reduce approximate relative error to 1.0. The level of error is within what would be expected given uncertainties in threshold shear velocity and windspeed at our sites. The model outperforms the alternative schemes both in terms of approximate relative error as well as the number of sites at which threshold shear velocity was exceeded. These results lend support to an understanding of the physics of aeolian transport in which vegetation's impact on transport is 1) dependent upon the distribution of vegetation rather than merely its average lateral cover, and 2) in which vegetation impacts surface shear stress locally by depressing it in the immediate lee of plants rather than by changing the bulk surface's threshold shear velocity. Our results also highlight the lack of understanding of how threshold shear velocity changes with space and time in real landscapes by suggesting that threshold is exceeded more than might be estimated by single measurements of threshold shear stress and roughness lengths commonly associated with vegetated surfaces.

Okin, G. S. (2008), A new model of wind erosion in the presence of vegetation, *J. Geophys. Res.*, 113: F02S10, doi: 10.1029/2007JF000758.

Notation

A	Equation (1) fitting constant, m^{-2}.
A	Constant present in equations for $Q_{x/h}^{u_*}$.
A_B	Average area of a single vegetation element (plant) projected onto the ground (i.e. basal area), m^2.
A_P	Average area of a single vegetation element (plant) projected onto a plane perpendicular to the ground (i.e. profile area), m^2.
b	Equation (1) fitting constant, m^{-1}.
β	Ratio of drag coefficient for vegetation to drag coefficient for ground [β = 202, *Shao*, 2008 p. 307]
c	Equation (1) fitting constant, g m^{-2} d^{-1}.
C	*e*-folding distance for the recovery of u_{*s} in the lee of a plant as it approaches u_*.
δ	Constant. δ=0 when $u_* < u_{*_t}$ and δ=1 when $u_* > u_{*_t}$.
$\overline{D}$	Average plant diameter, m.
D_P	Particle size diameter, used in MAR model, m.
EF	Erodible fraction used in RWEQ model.
ε_r	Approximate relative error of model estimates.
f_{eff}	Drag partition coefficient [*Marticorena et al*., 1997b].
f_{eff,z_1}	Drag partition coefficient induced by soil surface roughness [*Marticorena et al*., 1997b].
f_{eff,z_2}	Drag partition coefficient induced by soil vegetation [*Marticorena et al*., 1997b].
F_g	Fraction of the ground that is covered by plants.
g	Acceleration due to gravity, m s^{-2}.
h	Plant height, measured as Frisbee™ drop height, m.
K	Von Karman's constant, 0.4.
K'	Soil roughness factor used in RWEQ model.
$\overline{L}$	Average size of unvegetated gaps between plants, m.
λ	Lateral cover
m	Empirical parameter [*Raupach et al*., 1993].
n	Number of field sites.
$P_d(x/h)$	Probability that a point on the landscape is distance from the nearest upwind plant measured as *x/h*.
P_U	Probability distribution of windspeeds, *U*, during measurement period.
$Q_{t,\,act}$	Field-estimated horizontal flux, g m^{-1} d^{-1}.
$Q_{t,\,corr}$	Empirically-corrected model-estimated horizontal flux, g m^{-1} d^{-1}.
$Q_{t,\,pred}$	Model-estimated horizontal flux, g m^{-1} d^{-1}.
$Q_t^{u_*}$	Model-estimated horizontal flux at shear velocity, u_*, g m^{-1} d^{-1}.
$Q_{x/h}^{u_*}$	Horizontal flux at shear velocity u_* and distance from nearest upwind plant measured as x/*h*, g m^{-1} d^{-1}.
$q(z)$	Time-averaged horizontal flux density at height z above the surface,

	measured with a BSNE, g m^{-2} d^{-1}.
ρ	Density of air, g m^{-3}.
RMSEL	Root mean squared error of the logs of horizontal flux.
σ	Ratio of roughness-element basal area to frontal area, A_B/A_P.
SCF	Soil crust factor used in RWEQ model.
SD	Soil snow cover correction in the RWEQ model.
SLR_C	Soil loss ratio correcting for the growing plant canopy cover in the RWEQ model.
SLR_F	Soil loss ratio correcting for flat residue in the RWEQ model.
SLR_S	Soil loss ratio correcting for the plant silhouette in the RWEQ model.
SW	Soil wetness correction in the RWEQ model.
U_t	Threshold wind speed at 2 m in the RWEQ model, m s^{-1}.
U_z	Horizontal windspeed at height z, m s^{-1}.
u_*	Shear velocity of the wind, m s^{-1}.
u_{*S}	Shear velocity in the lee of a plant (as a function of *x/h*), m s^{-1}.
$\left(\frac{u_{*S}}{u_*}\right)_{x=0}$	Ratio of shear velocity in the immediate lee of a plant (x = 0) to shear velocity as estimated with the Law of the Wall.
u_{*t}	Threshold shear velocity of the soil, m s^{-1}.
u_{*tv}	Threshold shear velocity of the surface in the presence of vegetation [*Marticorena et al*., 1997b] and [*Shao*,2008], m s^{-1}.
$\overline{W}$	Average plant width along a transect, equal to $\pi/4\ \overline{D}$ for circular plants, m.
WF	Weather factor in RWEQ model, g m^{-1} d^{-1}.
x	Distance to nearest upwind plant, m.
x/h	Distance to nearest upwind plant measured as distance, *x*, scaled by plant height, *h*.
X_1	Reciprocal of distance between soil roughness elements [*Marticorena et al*., 1997b], set to 0.1, m.
X_2	One-third of the distance between plants [*Marticorena et al*., 1997b], m.
Y	Regression-derived value of Q_t in Equation (10), g m^{-1} d^{-1}.
z	Height above ground surface, m.
z_o	Aerodynamic roughness length, m.
$z_{o,1}$	Aerodynamic roughness length induced by soil surface [*Marticorena et al*., 1997b], m.
$z_{o,2}$	Aerodynamic roughness length induced by [*Marticorena et al*., 1997b], m.
z_{os}	Aerodynamic roughness length for a smooth surface, 10^{-5} m, [*Marticorena et al*., 1997b], m.

1. Introduction

Aeolian transport is a fundamental process in world's drylands, and it has direct impacts on climate, ecosystem dynamics, soil biogeochemical cycling, snow accumulation and melt, precipitation runoff, and public safety/health [*Sokolik and Toon*, 1996; *Li et al.*, 2007, Li *et al.*, 2008, *Reynolds et al.*, 2001; *Painter et al.*, 2007, *Painter et al.*, 2010; *Griffin et al.*, 2001]. Most aeolian transport occurs in arid and semiarid lands that cover nearly 40% of the land surface in the United States [*Reynolds and Stafford Smith*, 2002]. A report by *Seager et al.* [2007] predicts reduced soil moisture and increasingly arid conditions in the next decades over large areas of the arid Southwest Unites States and other studies have predicted aridification elsewhere [e.g., *Thomas et al.*, 2005]. The ability to estimate aeolian activity from process-based models is important for predicting future changes in aeolian activity given expected changes in climate, vegetation, and land use in the world's drylands. This is particularly true given the difficulty of measuring aeolian transport at the large scales that characterize the world's rangelands (rangeland is the most common form of land use in drylands).

Aeolian transport is strongly affected by non-erodible roughness elements such as immobile clasts and vegetation [*Lancaster and Baas*, 1998; *Tegen et al.*, 2002; *Gillies et al.*, 2006] that absorb a portion of the shear stress exerted by the wind. The amount of roughness encountered by the wind has been most widely quantified by an index of "lateral cover", λ, which is defined as the average frontal area of plants projected onto a plane perpendicular to both the ground surface and direction of the wind multiplied by their number density. Since *Marshall* [1971], lateral cover has been the primary parameter representing the amount of vegetation in shear stress partitioning models [e.g., *Marticorena et al.*, 1997 ; *Raupach*, 1992] and subsequent models for wind erosion and dust emission on vegetated surfaces [e.g. *Marticorena and Bergametti*, 1995; *Mahowald et al.*, 2002; *Zender et al.*, 2003]. Application of the *Raupach* [1992] shear stress partitioning model does lead to shear stress ratios (i.e. the ratio of shear stress on the soil to the total shear stress) that are consistent with experimental results [*King et al.*, 2005]. However, this model estimates threshold shear velocity in the presence of vegetation

[*Raupach et al.*, 1993] that are too high to produce horizontal flux given normal erosive winds when the lateral cover is greater than about 0.1 [*Okin*, 2008]. Field experiments, including those of *Lancaster and Baas* [1998] in Owens Valley, *Li et al.* [2007] in the Chihuahuan Desert (Figure 1), and *Belnap et al.* [2009] on the Colorado Plateau, in contrast, show that significant flux occurs even at relatively high lateral cover values.

Okin [2008] pointed out that the discrepancy between aeolian transport using lateral cover [e.g., *Marticorena et al.*, 1997 ; *Raupach*, 1992] and fluxes potentially results from the requirement that threshold shear velocity be the same everywhere. Conceptually, this is due to the fact that lateral cover only provides information on the density of vegetation but says nothing about how that vegetation is distributed and therefore the model can provide only estimates of the surface stress averaged over the exposed soil area. This issue was identified originally by *Raupach et al.* [1993], who introduced an empirical parameter (the *m* parameter) that was intended to adjust the lateral cover so that surface stress could be given by the maximum surface stress on the exposed soil area rather than the surface stress averaged over the exposed soil area.

Field observations have shown that horizontal sediment flux can be strongly affected by the spatial distribution of vegetation [*Okin and Gillette*, 2001; *Gillette et al.*, 2006]. Recently, *Okin* [2008] developed a new aeolian transport model using the distribution of erodible gaps between plants to characterize shear stress partitioning and distribution of shear stress at the soil surface. This new model provides very good estimates of shear stress ratios compared to laboratory and field experiments. In addition, it predicts horizontal flux in vegetation with relatively high densities ($\lambda > 0.1$), consistent with field observations (e.g. Figure 1). It does so by not requiring the flux occur at all points in the landscape at the same time; some areas protected by vegetation can be below threshold while more exposed area can be above threshold.

The purpose of this paper is to evaluate the *Okin* [2008] model of aeolian transport in the presence of vegetation (hereafter referred to as OK) and to estimate the best values for its parameters. Our strategy was to collect vegetation, soil, and meteorological data for as many as possible wind erodible sites where aeolian transport was actively monitored at the time of the research. Measured aeolian fluxes were then tested against modeled values to evaluate the model performance, to obtain a set of optimum model parameters, and to estimate the uncertainty in these parameters. The same field data were used to model horizontal flux using other schemes, including those of the Revised Wind Erosion Equation (RWEQ) [*Fryrear et al.*, 1998], *Marticorena et al.* [1997], and *Shao* [2008 p. 307], slightly modified so that their treatment of vegetation can be directly compared to that of the OK model using the same dataset. One purpose of this research is simply to prove a model that can be used to predict horizontal aeolian transport in real, structurally complex vegetation. A further, more critical goal is to determine whether treatment of vegetated landscapes in a way in which aeolian transport can occur in some exposed areas and not in other more protected areas (i.e., rather than requiring the entire landscape to have a single threshold), which is a more realistic picture of the physics of aeolian transport in vegetated landscapes, provides significantly better numerical predictions of aeolian transport when compared to other approaches.

2. Methods and Data

2.1. Description of the Sites

Our field sites were located in Utah, New Mexico, and California (Table 1). These sites represent all of the known actively monitored wind erosion sites in the western United States at the time this project was conducted. None of these sites were established for the purpose of conducting model evaluation. Because sites were established for other reasons, some measurements that would have been helpful for this study, especially meteorological observations near flux measurements, were not available and alternative, nearby observations had to be used instead. Evaluation of the impact of the uncertainty in meteorological observations is discussed below.

At each site, horizontal aeolian transport was monitored by a set of samplers ("stems") utilizing Big Spring Number Eight (BSNE) aeolian sediment traps [*Fryrear*, 1986]. A total of 65 BSNE stems were found that met the following criteria: 1) each BSNE stem was equipped with at least 3 traps; and 2) the mass of windblown sediment collected in the BSNE traps monotonically decreased with the increase of trap height. The latter criterion suggests that the sediment in traps is not dominated by non-local sources [*Bergametti and Gillette*, 2010]. The heights of the arithmetic center of the openings of the BSNE traps were recorded. The lowest traps were located ~0.1-0.15 m above ground surface and the top traps were mounted at about 1 m high. The deployment periods for the BSNE stems varied at different sites (Table 1), and windblown sediments were collected at the end of the experimental period.

For the Fivemile Mountain sites in Utah, shrubs were either removed or thinned by different mechanical treatments that varied in their effects on soil stability, vegetation structure, and the amount and distribution of residual woody debris. BSNE stems on the Clear Spot Flat sites were mostly located on lands burned by a severe wildfire in July 2007 and subsequently seeded using mechanical techniques that impacted soil erodibility. At the Jornada Experimental Range (JER), BSNE stems were located in a grassland with various levels of vegetation removal [*Li et al.*, 2007]. The reduced vegetation cover at the JER sites has been maintained since their establishment in summer, 2004.

2.2 Additional *in situ* Data Collection and Processing

At each BSNE stem site, fractional (foliar) vegetation cover and distribution of gaps were measured using a modified version of Standard NRCS National Resources Inventory Methods [*Herrick et al.*, 2005] (Table 2). At non-JER sites, all measurements were conducted along three 50-m transects oriented at 100, 220, and 340 degrees from due north and set up beginning 5 m from the BSNE stem. At the JER sites, measurements were conducted along three 50-m transects oriented in the direction of the prevailing wind. For inter-canopy gap measurements, only perennials and persistent woody debris from dead trees/shrubs were counted as gap stoppers and a minimum gap size was set as 20 cm. For each span of canopy between two gaps, canopy heights were determined by measuring the height of the center of a Frisbee™ (186 g, with a hole in the center) dropped along a meter stick from a height of 10 cm above the maximum canopy height. This empirical approach was used to approximate the effect of wind shear stress bending the top of the plants and to eliminate the effect of small/thin leaves or stems that may protrude significantly from the main canopy, but which probably have little impact on airflow. A distribution of scaled gap sizes was calculated as the ratio between a gap (cm) and the adjacent plant canopy height (Frisbee dropped height, cm) for all gaps and canopies along each of the transects. Subsequently, a histogram of the gap size, scaled by adjacent plant height, was constructed (Figure 2).

Threshold shear velocity (u_{*t}) for unvegetated soils (i.e., for the soil itself rather than the vegetated surface as a whole) was estimated using a method newly developed by *Li et al.* [2010]. In this method, u_{*t} was quantitatively related with the resistance of the soil surface to disturbances created by a penetrometer and projectile shot by an air gun at the soil. Briefly, at each BSNE stem, a total of 15 repeated air gun and penetrometer measurements were conducted along each transect starting from 5 m with an interval of 10 m. Both air gun and penetrometer were applied at 45 degrees to the soil surface, and the readings from the penetrometer and sizes of the surface soil disturbance (length × width) created by the air gun were recorded. Average values were used to evaluate a regression equation to estimate u_{*_t}.

Horizontal wind speed (*U*) data were obtained from on-site meteorological towers or wind towers located nearby and operated by other organizations (Table 1). The interval of the wind speed records varied from 5 min to up to 1 hr. Wind data used in modeling were compiled for each horizontal flux estimate for the same period of sample collection.

Total horizontal mass flux from the BSNEs ($Q_{t,act}$) was calculated based on the weight of sediments collected in each BSNE trap and their deployment time by using the method described in *Li et al.* [2007]. The mass of sediments collected in the BSNE traps was divided by the inlet area of the trap (1×10^{-3} m^2) and the time of the collection to obtain the time-averaged horizontal mass flux density $q(z)$ in g m^{-2} d^{-1}, where z is the height of the arithmetic center of the inlet above the ground (m). Values of $q(z)$ were fitted to an empirical formula [*Shao and Raupach*, 1992]:

$$q(z) = c\mathrm{Exp}\left(ah^2 + bh\right), \tag{1}$$

where a, b, and c are fitting constants. The values for total horizontal flux $Q_{t,\,act}$ were calculated by:

$$Q_{t,act} = \int_{0\ \mathrm{m}}^{1\ \mathrm{m}} q(z)dz \;. \tag{2}$$

The maximum height of integration was set to 1 m because only a small percentage of the flux (generally less than 10%) occurs at heights >1 m [*Li et al.*, 2007].

2.3 Description of the Model

The details of the wind erosion model have been described by *Okin* [2008]. In brief, prediction of the horizontal flux $Q_t^{u_*}$ (expressed in units of mass per unit distance perpendicular to both the wind and the ground per unit time) for a specific wind shear velocity, u_* (m s^{-1}), is achieved by modeling the distribution of gaps downwind of plant canopies as:

$$Q_t^{u_*} = (1 - F_g) \int_0^{\infty} Q_{x/h}^{u_*} P_d(x/h) d(x/h), \tag{3}$$

where F_g is the ground fraction that is covered by vegetation, x is a distance from the nearest upwind plant (m), h is the height of that plant (m), $Q_{x/h}^{u_*}$ is the horizontal flux (g m^{-1} d^{-1}) for a point x/h away from the nearest upwind plant at the shear velocity, u_*, and $P_d(x/h)$ is the probability that any point in the landscape is a certain distance from the nearest upwind plant expressed in units of height of that plant. The overall horizontal flux ($Q_{t,pred}$) for all wind speeds is calculated by:

$$Q_{t,pred} = \int_0^{\infty} P_{u_*} Q_t^{u_*} du_* . \tag{4}$$

In the OK model as originally published, horizontal flux at a certain point, $Q_{x/h}^{u_*}$, is calculated using the formulation of *Owen* [1964] and re-defined by *Shao et al.* [1993] and *Gillette and Chen* [2001]:

$$Q_{x/h}^{u_*} = A \frac{\rho}{g} u_* (u_*^2 - u_{*t}^2) \delta, \tag{5}$$

where A is a unitless constant that may vary between 0 and 1, ρ is the density of air (g m^{-3}), g is the acceleration due to gravity (m s^{-2}), and u_{*_t} is the threshold shear velocity of the unvegetated soil (m/s), δ is a constant with δ=0 when $u_* < u_{*_t}$ and δ=1 when $u_* > u_{*_t}$.

The OK model assumes each plant is associated with a reduced shear stress wake zone and this zone of reduced shear stress is described by an exponential curve:

$$u_{*s} = u_*\left(\left(\frac{u_{*s}}{u_*}\right)_{x=0} + \left[1-\left(\frac{u_{*s}}{u_*}\right)_{x=0}\right]\left[1-e^{-C(x/h)}\right]\right), \tag{6}$$

where u_{*s} is the shear velocity downwind of plant, $\left(\frac{u_{*s}}{u_*}\right)_{x=0}$ is the value of u_{*s}/u_* in the immediate lee of a plant, and C is the e-folding distance for recovery of the shear velocity in the lee of plants (that is, C is the exponential constant that describes the rate, in units of plant height, h, at which the shear velocity, u_{*s}, recovers to the value it would have in the absence of vegetation, u_*). The physical meaning of these parameters is summarized in Table 3.

In the model, u_* is related to the mean wind speed, U, at height z (cm) by a rearranged form of Law of the Wall:

$$u_* = UK \Big/ \ln\left(\frac{z}{z_0}\right), \tag{7}$$

where K is von Karman's constant (K = 0.4), and z_o is aerodynamic roughness length (m).

At the scale of many wind erosion models, the parameter roughness length (z_o) varies over heterogeneous landscapes as it is related to both plant lateral cover and canopy height [e.g., *Marticorena et al.*, 1997a]. In the OK model, z_o is set as a constant for all sites. This allowed us to treat z_o as a fitting parameter in our model validation and meant that z_o would not have to be estimated at each field site. Other model input parameters, including A, C, and $\left(\frac{u_{*s}}{u_*}\right)_{x=0}$, were also treated as constant for the purpose of the model validation. In the OK model, the impact of the shrub structure is accounted for mostly in the $\left(\frac{u_{*s}}{u_*}\right)_{x=0}$ parameter. In reality, to some extent the vegetation structure will impact shear stress partitioning and therefore $\left(\frac{u_{*s}}{u_*}\right)_{x=0}$, but there is in fact a remarkable degree of overlap in shear stress portioning ratio (SSR) amongst solid and porous objects [*King et al.*, 2005]. When examining all available SSR in light of the OK model, there was no clear value of $\left(\frac{u_{*s}}{u_*}\right)_{x=0}$ that separated solid from porous objects, although there was a slight bias toward higher values of $\left(\frac{u_{*s}}{u_*}\right)_{x=0}$ for porous objects. In light of these observations, it is unclear how much $\left(\frac{u_{*s}}{u_*}\right)_{x=0}$ would vary amongst porous objects. In short, there is no compelling reason based on existing data to treat $\left(\frac{u_{*s}}{u_*}\right)_{x=0}$ as anything but a bulk constant. C, too, may vary with shrub structure or porosity, but in the absence of experimental or theoretical guidance on this and for the purpose of parsimony, it has been treated as a constant.

In recognition of the fact that z_o does change with vegetation density, a modified version of the *Okin* [2008] model (hereafter called the "modified *Okin* [2008] model", or MOK) was also implemented. In this modified model, aerodynamic roughness length was allowed to vary as a function of lateral cover, using the approach of *Marticorena et al.* [1997] as presented by *Shao* [2008 p. 318], with additional modifications. First, z_o was calculated using:

$$z_o = \begin{cases} (0.48\,\lambda + 0.001)h & \lambda < 0.11 \\ 0.0538\,h & \lambda \geq 0.11 \end{cases}. \qquad (8)$$

Okin [2008] showed that lateral cover, λ, was related to average gap size by:

$$\lambda = \frac{A_P \overline{W}}{A_{B\left(\overline{L}+\overline{W}\right)}}, \tag{9}$$

where A_P is the profile area of a plant, A_B is the basal area of plant, $\overline{L}$ is the average size of unvegetated gaps between plants, and $\overline{W}$ is the average width of a plant along a transect (equal to π/4 of the plant diameter, $\overline{D}$, for circular plants). The fractional cover of plant, F_g, is given, in these terms, by:

$$F_g = \frac{\overline{W}}{\overline{L}+\overline{W}}, \tag{10}$$

Assuming cylindrical geometry (i.e. $A_B = \pi/4\,\overline{D}^2$ and $A_P = \overline{D}h$) it can be shown that

$$\lambda = \left(1 - F_g\right)\frac{h}{\overline{L}}. \tag{11}$$

Initial tests using Equation (8) for aerodynamic roughness length alone showed that for field sites without vegetation cover the model produced no flux because z_o was too low and resulting u_* never exceeded u_{*t}. This is in direct contradiction with our field measurements; bare sites did produce significant horizontal flux. So, a modified aerodynamic roughness length, z'_o, was used in MOK instead of z_o calculated from Equation (8). Specifically, a linear relationship was applied that adjusted all roughness values:

$$z'_o = z_{o,\min} + z_o\left(\frac{z_{o,tie} - z_{o,\min}}{z_{o,tie}}\right), \tag{12}$$

where $z_{o,min}$ is the minimum value for z'_o and was set to 0.01 m, and $z_{o,tie}$ was set to 0.1 m (Figure 3).

In this study, several different horizontal flux equations were tried in place of Equation (5) in both the OK and MOK models. Over the past few decades, many experimental and numerical studies have investigated the variation of horizontal mass flux with shear velocity. These studies have led to different equations but predominantly with the form that $Q_{t,\ pred}$ scales with approximately the third power of the shear velocity. We tested the model performance in combination with the horizontal mass flux equations in Table 4. For the OK model, the best equation was identified, together with the set of model parameters: z_o, A, C, and $\left(\frac{u_{*s}}{u_*}\right)_{x=0}$. For the MOK model, the best equation was identified, together with the set of model parameters: A, C, and $\left(\frac{u_{*s}}{u_*}\right)_{x=0}$.

2.4 Parameter Estimation and Cross Validation

An algorithm aimed at finding the global minimum error was employed. Random values of log[A], C, $\left(\frac{u_{*s}}{u_*}\right)_{x=0}$, and log[$z_o$] (for OK) were chosen from uniform distributions bounded by physically reasonable values of each of the parameters (Table 5). Predicted values of $Q_{t,pred}$ were calculated for all BSNE stems used in the minimization, and the root mean squared error of the logs (*RMSEL*) was calculated as:

$$RMSEL = \left(\frac{1}{N} \sum_N \left(Log(Q_{t,pred}) - Log(Q_{t,act}) \right) \right)^{1/2}, \tag{13}$$

where $Q_{t,pred}$ is the predicted value of horizontal flux using the randomly selected parameter values, $Q_{t,act}$ is the value of horizontal flux estimated from the BSNE stems, and N is the number of BSNEs used in the minimization. A small constant (<< minimum($Q_{t,act}$)) was added to both $Q_{t,pred}$ and $Q_{t,act}$ to prevent values of negative infinity if either equals zero. This was done 1,000 times and the set of parameters that yielded the lowest *RMSEL* was chosen as the best-fit set of parameters.

This iterative process was conducted 65 times. Each time, 64 sites were used in the error minimization, while one was left out (i.e., each site was left out once). The final *RMSEL* was calculated using Equation (13), but substituting the predicted values for the omitted site as $Q_{t,pred}$ and the actual horizontal flux values of the omitted site as $Q_{t,act}$. This parametric leave-one-out (LOO) cross-validation analysis was conducted to provide mean estimates of key model parameters and was done for every flux equation in Table 4.

Error estimation and model comparison is further discussed below.

2.5. Empirical Model Improvement by Stepwise Regression of Residuals

Although the main goal of this study was to validate the process-based OK, additional steps were taken after the best-fit flux equation and model parameters were determined. From this best model, a stepwise regression was conducted on residuals in log space:

$$residual = Log(Q_{t,act}) - Log(Q_{t,pred}). \tag{14}$$

In this process, the field-derived parameter that had the highest absolute correlation (i.e., $|r|$) with $Q_{t,act}$ was determined and residuals were regressed against this parameter. A correction was then calculated based on this regression:

$$Log(Q_{t,corr}) = Log(Q_{t,pred}) + Y, \tag{15}$$

where Log($Q_{t,corr}$) is the regression-corrected value of Log($Q_{t,pred}$) and Y is the value given by the regression equation. Next, the field-derived parameter with the highest $|r|$ with the remaining residual, calculated with Log($Q_{t,corr}$) replacing Log($Q_{t,pred}$) in equation (14), was identified and a regression of the remaining residual against both field-derived parameters was conducted. New corrected values of Log($Q_{t,corr}$) were calculated using this multiple regression. This process was repeated until little reduction of RMSEL was obtained with the addition of a new parameter. In addition, the single regression corrections using each of the two field-derived parameters with the highest $|r|$ were investigated (that is, rather than simply the sequential approach described above).

2.6 Sensitivity of errors to uncertainty in site parameters

To determine the effect that uncertainty in the plot-level parameter values (u_{*t}, mean wind speed, mean scaled gap size, and vegetation cover) might have in overall model performance, a series of simulations were conducted. For all 65 sites used in this study, model predictions of horizontal flux were made, using the *Gillette and Passi* [1988] flux equation and final fitting parameters, and plot-level parameters for that site. The choice of flux equation here should not impact the interpretation of these results. Wind speed distribution was estimated as a Weibull distribution [*Gillette and Passi*, 1988] with a shape parameter equal to two and mean equal to that measured at the tower closest to the site. These model predictions were set as reference values ($Q_{t,act}$).

Next, 100 new predictions were made ($Q_{t,pred}$), drawing the values of threshold shear velocity (u_{*t}), and mean wind speed for each iteration from normal distributions with means equal to the measured value at each site and a given coefficient of variation (CV). Error (see section 2.8) was calculated for the set of predictions. Values of the CV for both variables were 0.05, 0.10, 0.15, 0.20, and 0.25. All combinations of CV for both variables were used resulting in 25 (5^2) estimates of error. CV for fractional cover and mean scaled gap size was set to be 5% because they were found to not contribute significantly to the total error.

2.7 Other Models

Field data were used to parameterize three additional models of the impact of vegetation upon horizontal sediment flux: the *Marticorena et al.* [1997] (hereafter MAR) model, the *Shao* [2008] model (hereafter SHAO), and the Revised Wind Erosion Equation [RWEQ, *Fryrear et al.*, 1998]. Because the OK model is fundamentally a model of how vegetation impacts horizontal flux, only those portions of MAR, SHAO, and RWEQ that pertain to the effect of vegetation upon horizontal flux were implemented. That is to say, to provide the most reasonable basis of comparison, threshold shear velocity for the soil (i.e. without the effect of vegetation) in all model calculations was set to that measured in the field. In the RWEQ and SHAO model, where there are multiple factors related to soil that were not measured, these were set to constant values to allow a consistent basis of comparison.

2.7.1 *Marticorena et al.* [1997] model, MAR

The basic flux equation for the MAR model is:

$$Q_{tot,pred} = (1-F_g)A\frac{\rho}{g}\sum_{u_*} u_*^3 \int_{D_P}\left(1+\frac{u_{*tv}}{u_*}\right)\left(1-\left(\frac{u_{*tv}}{u_*}\right)^2\right)dD_P, \qquad (16)$$

where D_p is the particle diameter and u_{*tv} is given by:

$$u_{*tv} = \frac{u_{*t}}{f_{eff}}. \qquad (17)$$

In the model as originally published, u_{*t} is evaluated for each particle size. Here, u_{*t} is set to that measured in the field and therefore (16) simplifies to:

$$Q_{t,pred} = (1-F_g)A\frac{\rho}{g}\sum_{u_*} u_*^3\left(1+\frac{u_{*tv}}{u_*}\right)\left(1-\left(\frac{u_{*tv}}{u_*}\right)^2\right). \qquad (18)$$

For a surface with vegetation:

$$f_{eff} = f_{eff,z_1} f_{eff,z_2}, \qquad (19)$$

where f_{eff,z_1} accounts for the roughness of the rough soil surface and f_{eff,z_2} accounts for the roughness provided by the vegetation. In the absence of vegetation f_{eff} is calculated as f_{eff,z_1} only.

f_{eff,z_1} is given by:

$$f_{eff,z_1} = 1 - \left(\ln\left(\frac{z_{o,1}}{z_{os}}\right)\right)\left(\ln\left(0.35\left(\frac{X_1}{z_{os}}\right)^{0.8}\right)\right)^{-1}, \tag{20}$$

where z_{os} is the roughness length of the smooth surface [set to 10-5 m, *Marticorena et al.*, 1997], X_1 is the distance between soil roughness elements [set to 0.1 m, *Marticorena et al.*, 1997], and $z_{o,1}$ is the roughness length imparted by the soil roughness. $z_{o,1}$ was set to 5.38×10^{-4} m, which is consistent with lateral cover of soil roughness elements ≥ 0.11 and soil roughness elements one cm in height (see Equation (8)).

f_{eff,z_2} is given by:

$$f_{eff,z_2} = 1 - \left(\ln\left(\frac{z_{o,2}}{z_{o,1}}\right)\right)\left(\ln\left(0.35\left(\frac{X_2}{z_{o,1}}\right)^{0.8}\right)\right)^{-1}, \tag{21}$$

where $z_{o,2}$ is the roughness length imparted by the vegetation and X_2 is one-third the distance between plants and can be calculated from our field data calculated by $(\overline{L}+0.5\overline{W})/3$. $z_{o,2}$ was calculated using Equation (8).

For the implementation of the MAR model here, u_* was determined using Equation (7) and $z_{o,2}$, or in the absence of vegetation, $z_{o,1}$.

2.7.2 *Shao* [2008] model, SHAO

The basic flux equation for the SHAO model is:

$$Q_{tot,pred} = (1-F_g)A\frac{\rho}{g}\sum_{u_*} u_*^3 \int_{D_P}\left(1-\left(\frac{u_{*tv}}{u_*}\right)^2\right)dD_P, \tag{22}$$

u_{*tv} is given by:

$$u_{*tv} = \frac{u_{*t}}{\sqrt{(1-m\sigma\beta)(1+m\beta\lambda)}}, \tag{23}$$

where u_{*t} is evaluated for each particle size, m is an empirical constant [m = 0.16, *Shao*, 2008 p. 307], and β is the ratio of element to surface drag coefficients [β = 202, *Shao*, 2008 p. 307]. $\sigma = A_B/A_P$, and is given by *Shao* [2008] as a constant, but can be calculated from our field data assuming cylindrical plant geometry (i.e. $A_B = \pi/4\,\overline{D}^2$ and $A_P = \overline{D}h$). In the original SHAO model, u_{*tv} also had corrections for soil moisture, salt concentration and surface crust. Since we had direct measurements of u_{*t}, these were not used (i.e., were set to one), nor was the dependence upon grain size used. Therefore, Equation (22) simplifies to:

$$Q_{t,pred} = (1 - F_g) A \frac{\rho}{g} \sum_{u_*} u_*^3 \left(1 - \left(\frac{u_{*tv}}{u_*} \right)^2 \right), \quad (24)$$

u_* was determined using Equation (7) with z_o calculated from Equation (8) using lateral cover calculated from Equation (9).

2.7.3 Revised Wind Erosion Equation (RWEQ)

The RWEQ model calculates horizontal transport as it increases across an agricultural field toward maximum value. This maximum value was used here as the main point of comparison:

$$Q_{t,pred} = 0.1098 \cdot WF \cdot EF \cdot SCF \cdot K' \cdot SLR_F \cdot SLR_S \cdot SLR_C\,, \quad (25)$$

where WF is the weather factor (g m^{-1} d^{-1}), EF is the erodible fraction (unitless), SCF is the soil crust factor (unitless), K' is the soil roughness factor (unitless), SLR_F is the soil loss ratio for flat cover (unitless), SLR_S is the soil loss ratio for plant silhouette (unitless), SLR_C is the soil loss ratio for growing plant canopy (unitless). WF is given by:

$$WF = 4.8x10^{-2} \frac{\rho}{g} \sum_{U_2} U_2 (U_2 - U_t)^2 \cdot SW \cdot SD, \quad (26)$$

where U_2 is the windspeed (m s^{-1}) at 2 meters and U_t is the threshold windspeed (m s^{-1}) at 2 meters. *SW* is a factor that corrects for soil wetness and *SD* is a factor that corrects for snow cover; both were set to one. The coefficient 4.8 $\times 10^{-2}$ includes both an empirical factor (1/500) and corrections to yield units of g m^{-1} d^{-1} for consistency with the other models in this application. Windspeed at 2 m was calculated using measured windspeed at height z, U_z:

$$U_2 = U_z \frac{\ln(2/z_o)}{\ln(z/z_o)}, \quad (27)$$

where z_o was calculated using Equation (8). Threshold windspeed at 2 m, U_t, was calculated as:

$$U_t = \frac{u_{*t}}{K} \ln\left(\frac{2}{z_o}\right). \quad (28)$$

EF is a complicated function of soil texture:

$$EF = \frac{1}{100}\left(29.09 + 0.31\%sand + 0.17\%silt + 0.33(\%sand/\%clay) - 0.259\%organicmatter - 0.95\%CaCO_3\right). \quad (29)$$

Texture data was not available, so the maximum possible value of EF (0.630) was calculated using the soil parameters given in *Fryrear et al.* [1998]: 0.18% organic matter, 93.6% sand, 0.5% silt, 5.9% clay, 0% $CaCO_3$. Using these same soil parameters, *SCF*, given by:

$$SCF = \left(1 + 0.0066(\%clay)^2 + 0.021(\%organicmatter)^2\right)^{-1}, \quad (30)$$

was calculated as 0.813, which is close to the highest value reported by *Fryrear et al.* [1998], 0.823. K' is a correction for soil random roughness, which was not measured, so it was set to its maximum value, 1.0, which corresponds to a rough soil. SLR_F corrects for the amount of flat plant residue on the surface, which we assumed to be zero because our field sites weren't agricultural fields with residue, and was therefore set to 1.0. SLR_S is given by:

$$SLR_S = Exp\left(-0.344\lambda^{0.6413}\right). \quad (31)$$

SLR_C corrects for the amount of soil covered by plants, i.e. (1-F_g), and is given by:

$$SLR_S = Exp\left(-0.5614 F_g^{\ 0.7366}\right). \quad (32)$$

For the RWEQ model, maximum values of soil parameters (SD, SW, *EF*, *SCF*, and *K'*) were set as constants to obtain a consistent set of predictions for which soil conditions (except U_t) are common to all sites. Because the purpose of the using additional models' horizontal flux predictions in this report is to compare how they treat vegetation with respect to how the OK model treats vegetation, the use of constant values for soil parameters is justified. This is particularly true with the RWEQ model because of the linear way in which these parameters are included in the flux equation (i.e., Equation (25)).

2.8 Error Metrics and Model Comparison

The *RMSEL* was utilized instead of the root mean squared error (*RMSE*, the error calculated without first taking the log) because the horizontal flux estimates spanned two orders of magnitude. The use of *RMSEL* instead of *RMSE* is justified by the purpose of the OK model, which is to estimate horizontal over a wide range of field conditions including those with low flux. The use of *RMSE* would emphasize errors of prediction for larger fluxes considerably more than errors of prediction for smaller fluxes because the same relative error in the both cases yields a larger error in the case of the larger flux. It is our contention that locations with higher horizontal transport are not necessarily more meaningful in terms of the total amount of transport in or dust produced from natural landscapes. This is particularly true when the potential for horizontal aeolian transport to produce atmospheric dust is considered. The amount of dust produced from landscapes (i.e., the vertical flux in units of M A^{-1} T^{-1}) can be approximated as a linear function of the horizontal flux with the constant of proportionality, the dust production efficiency, depending on soil characteristics [e.g., *Gillette*, 1977]. Therefore the amount of dust produced from a landscape is the product of the horizontal flux, the area over which the horizontal flux occurs, and the dust production efficiency. That is to say, large areas with relatively low flux may produce as much dust as small areas with higher flux. With this in mind, it would seem necessary to have a model that can estimate both the small fluxes and the large fluxes equally well. Thus, we chose to use as our error metric RMSEL, which emphasizes error for small fluxes and large fluxes equally, over RMSE, which emphasizes error for large fluxes over small fluxes.

It can be shown that e^{RMSEL} is the geometric mean of the ratio of $Q_{t,pred}$ to $Q_{t,act}$. Because

$$Q_{t,pred} - Q_{t,act} = \varepsilon, \tag{33}$$

where ε is the absolute error, the ratio of $Q_{t,pred}$ to $Q_{t,act}$ can be expressed as

$$\frac{Q_{t,pred}}{Q_{t,act}} = 1 + \frac{\varepsilon}{Q_{t,act}}, \tag{34}$$

where $\varepsilon/Q_{t,act}$ is the relative error. e^{RMSEL} is the geometric mean of Equation (34) and thus, we propose as a metric of error, ε_r:

$$\varepsilon_r = e^{RMSEL} - 1 = \left\langle 1 + \frac{\varepsilon}{Q_{t,act}} \right\rangle - 1. \tag{35}$$

Although ε_r is not strictly equal to the relative error, it is an approximation of it with the property that it is equal to zero when there is no prediction error. ε_r values for the MAR, SHAO, and RWEQ models were calculated after correcting $Q_{t,\ act}$ from these models by the slope and intercept of their regression against $Q_{t,\ act}$.

3. Results

3.1 Characteristics of the Model Input Data and Horizontal Flux Estimates

Characteristics of model input data, including vegetation, threshold shear velocity, and wind are given in the Supplemental Materials Table S1. Bare sites were found in both Moab and

Clear Spot Flat, Utah, and the latter study site also had the largest average gap of 11 m. Average scaled gap (gap size/canopy height) ranged from 18 in the shrubland of Fivemile Mountain, UT to 282 in the burned Clear Spot Flat, Utah sites. Threshold shear velocity for unvegetated soil fell in the range of 0.19 to 1.04 m s^{-1}. During the experimental period, a large proportion of the windspeeds were lower than 5 m s^{-1} for all study sites, and peak windspeeds varied from 12 to over 26 m s^{-1}, observed in the Owens Valley, California site (Table 5, Figure 4).

The fit of $q(z)$ to Equation (1) generally gave very good fits (Table S1 in Supplementary Material). Coefficients of determination for these fits, r^2, are not particularly useful because many of the sites had only three BSNE traps on a stem and Equation (1) has three parameters, thus resulting in $r^2 = 1$. However, for sites with more than three BSNEs on a stem (i.e., all sites excluding the Utah sites) the fits are generally very good, with only two being fit with $r^2 > 0.9$. BSNE-estimated $Q_{t,act}$ spanned two orders of magnitude, with the greatest flux of 98 g m^{-1} d^{-1} found in a site in the Jornada Experimental Range, New Mexico, where grass cover had been removed (Figure 5). $Q_{t,act}$ was generally the lowest in the shrubby grassland of Owens Valley sites, despite the high windspeeds at these sites.

3.2. Model Evaluation

As expected, different mass flux equations (Table 4) yielded different best-fit values of key model parameters for the OK model (Table 6). The mean optimum values for the roughness length (z_o), e-folding distance for recovery of shear stress (C), and $\left(\frac{u_{*s}}{u_*}\right)_{x=0}$ ranged from 0.77-0.83 m, 5.6-6.2, and 0.28-0.32, respectively. The A constants have a variety of magnitudes due to the different forms of the mass flux equations. Uncertanty of the fits from the LOO cross-validation are small relative to parameter values, indicating confidence that the fitting procedure was stable and that these are the best predicted values of these parameters.

The performance of the OK model in combination with different mass flux equations was evaluated by regression of $Q_{t,pred}$ against $Q_{t,act}$ (Table 7). The regression equations generally had a slope close to 1 and a fairly small, positive intercept (0.019 to 0.069) except in the case of the modified *Shao et al.* [1993] flux equation. r ranged from 0.64 to 0.67 and ε_r ranged from 2.1-2.4, except for the modified *Shao et al.* [1993] flux equation for which ε_r was 6.0. The *Gillette and Passi* [1988] and *Sorensen* [1991] flux equations had the best and essentially the same values of r and ε_r for the OK model. Correction for those field-measured parameters with the highest correlation with residuals (median plant height, F_g, u_{*t}, and median windspeed) lowered ε_r to 1.0 for both flux equations (Table 8).

The MOK model, in which z_o was allowed to vary with lateral cover and plant height, did not perform as well as the original OK model, in which z_o was set to a constant for all data points. Values of C, and $\left(\frac{u_{*s}}{u_*}\right)_{x=0}$ were close to those found with the OK model, and A varied across several orders of magnitude in much the same pattern as the OK model (Table 9). r for $Q_{t,pred}$ from the MOK model with $Q_{t,act}$ were in the range 0.56-0.58 and values of ε_r were 3.0 – 3.6 for all flux equations except the modified *Shao et al.* [1993] equation, which had a very high ε_r of 33. In all, the *Gillette and Passi* [1988] flux equation provided the best estimates (lowest ε_r) for the MOK model (Table 10). Empirical corrections to the MOK model using this flux equation were able to reduce ε_r by about half, to 1.6 (Table 11).

Results from the uncertainty analysis show that minimum expected ε_r when both u_{*t} and median windspeed are known within 5% (i.e., when CV=0.05) is around 0.4 (Figure 6). Uncertainty in u_{*t} and mean wind speed of 25% leads to an expected ε_r ~7.

3.3. Other Models

Of the other models evaluated here, only RWEQ predicted flux for all 65 sites. The MAR model predicted flux for only three sites (i.e., no flux was predicted for 62 sites) and the SHAO model predicted flux for 38 sites (i.e. no flux was predicted for 27 sites). In comparison to these models, the OK model showed the highest value of r and the lowest value of ε_r, except for the MAR model.

4. Discussion

The present work uses a large number of sites (n = 65) over a wide geographic area with a variety of soil and vegetation types, and with temporal periods from four to five months (Tables 1, 5). The sites that were chosen for this study were all those that we could identify at the time of the research, and were not established for the purposes of this project. Aeolian activity was observed at all sites, only two of which were unvegetated (Table 1). In the present study, the OK-modeled values of $Q_{t,pred}$ were significantly correlated with $Q_{t,act}$ at the 99% level (r_{crit} < 0.325 [*Rohlf and Sokal*, 1981]) with approximate relative errors (ε_r) around 2-3, depending on flux equation, without empirical correction. With empirical correction, ε_r can be as low as 1.0 when all four field measures are incorporated (h, F_g, u_{*t}, and median windspeed), but the addition of just h and F_g can bring ε_r to 1.2-1.3. Although inclusion of median windspeed does improve model performance in terms of ε_r, it provides at best a small improvement. For the empirical correction, h, F_g, and u_{*t} can easily be estimated in the field, and therefore their use for empirical correction of model estimates should be straightforward in most cases. The fact that these parameters are significantly correlated to model error suggests that future improvements to the model should involve modifications related to these parameters.

The OK model, as originally conceived, treated z_o as a constant. It was thought that the z_o in the model was the roughness length due to the roughness of the soil alone. However, our estimation of model parameters shows in all cases that the best results are obtained when z_o is 0.07 – 0.08 m, which is the roughness length expected for vegetated surfaces rather than due to the soil roughness only. There are reliable published relationships between vegetation cover and z_o [e.g., *Marticorena et al.*, 1997], and a modification of the OK model was evaluated to determine whether taking into account vegetation roughness in the model might improve it. Although $Q_{t,pred}$ from this MOK model is still significantly correlated with $Q_{t,act}$, the correlations are lower (and the relative errors, ε_r, are higher) than the original OK model. In order to obtain even these results, the relationship for z_o had to be adjusted to increase roughness (Equation 12).

From a modeling perspective, the fact that the surface must be treated as if were rougher than the bare soil and also rougher than predicted from the published relationships between vegetation and z_o suggests one of two things under the long-term field measurement scenarios; either the surface really behaves as if it is rougher than expected or, u_{*t} behaves as if it is lower than expected. Because airflow over rough surfaces is better understood from theoretical considerations and laboratory experiments and is also more predictable than soil surface characteristics over extensive temporal and spatial scales, the latter explanation is more likely. This conclusion is independent of the OK or MOK treatment of vegetation. Consider, for example, two of our sites that were unvegetated. These sites experienced flux and had values of $Q_{t,act}$ in the middle of our measured range. Use of typical values for z_o for bare soil (<0.01 m) did not yield any times at which u_* exceeded u_{*t} even though the estimated u_{*t} values were not particularly high (u_{*t} = 0.48 and 0.71 m s^{-1}).

Our understanding of the physics of aeolian transport requires that, on certain temporal and spatial scales, transport can only occur when u_{*t} exceeds u_*. We do not refute this. Nevertheless, over spatially extensive real landscapes in which transport is measured over a period of several months, our results suggest that u_{*t} behaves as if it is lower than what is measured at a single time period. The values of u_{*t} used here were the minimum values measured at 10-m intervals extending 50-m outward from the BSNE stems. They should, therefore, provide a reasonable estimate of the minimum threshold in the area over which saltation flux may be expected to contribute to measured BSNE fluxes. But, these measurements were only taken at one time. Further research is required to understand how u_{*t} varies through time in natural landscapes experiencing aeolian transport. Until this discrepancy can be reconciled, our results suggest that adequate modeling results can be obtained by treating the surface as if it is rougher (i.e. greater z_o) than expected. Using a constant z_o, as in the OK model, provides a better fit to the observational data than a z_o that varies with vegetation density and height, as in the MOK model. For the sake of better predictions as well as model parsimony, the OK model should be preferred over the MOK model for the time being.

Our evaluation of the OK model shows that it compares quite favorably to other studies that have evaluated models of horizontal aeolian flux quantitatively in the field. *Van Pelt et al.* [2004] compared estimates of aeolian soil loss from bare fields around Big Springs, Texas, USA, for 41 events and modeled the flux using the RWEQ. Using the same method of error evaluation used here, we calculated an ε_r of 2.9. The RWEQ users guide published by *Fryrear et al.* [1998] provided data on measured and modeled flux at 51 agricultural fields for periods of several months that were used to calibrate the model. For the sites for which transport was predicted ($n = 49$), we calculate $\varepsilon_r = 4.6$. *Buschiazzo and Zobeck* [2008] measured 26 individual events on a bare field in the Argentine Pampas and compared these measurements with model estimates using the RWEQ and the stand-alone erosion submodel of the Wind Erosion Prediction System (WEPS). Both models underestimated flux by 45% and 40%, respectively. Because they did not report actual measured values in a table or easily-extractable figure format, it is impossible to conduct the same type of error evaluation used here, but taking the reciprocal of the underestimations gives 2.2 and 2.5, respectively, meaning that the models were within a factor of about 2.2 – 2.5 from field estimates, albeit systematically. For fields with cover under conventional and no-till agriculture fields in this same study, these two models failed to predict any sediment movement for all but one event despite observations of transport for over half of the events. For the events where flux was measured, flux was nonetheless high, averaging 6500 and 5000 g m^{-1} d^{-1} for conventional and no-till fields, respectively. *Feng and Sharratt* [2007] measured aeolian flux from fields (average cover = 50%) on a single soil type on the Columbia Plateau for six one-to-two week periods and compared these with estimates from WEPS. The model failed to predict any soil loss for half of the periods and significantly over predicted soil loss for the other three periods. In their study, the overall r between predicted and modeled soil loss values was 0.71, which is not statistically significant (α = 0.95, r_{crit} = 0.811, τ_{crit} = 0.867 [*Rohlf and Sokal*, 1981]). The fact that both the Buschiazzo and *Zobeck* [2008] and *Feng and Sharratt* [2009] studies had a considerable number of cases in which no flux was predicted despite being measured, particularly in the presence of vegetation, highlights the difficulty of simulating aeolian activity in the presence of vegetation. It is critical in these comparisons to note that all of the studies referenced above were from agricultural fields, many of them bare, and on which soil parameters could be measured in detail. All of the studies cited above except *Fryrear et al.* [1998] were also for individual storms. Bare soil or homogenous crop plantings and single events with on-site meteorological measurements are arguably much simpler systems for modeling aeolian transport than the structurally and spatially heterogeneous rangelands used in this study. In addition, the fact that there were several cases in which aeolian activity was not modeled, even though it was observed, constitutes a significant failure of these models. There are no such cases in the present study for the OK model and we believe that these comparisons show that the OK model performs well above benchmarks set by previous studies.

Using the extensive dataset collected for this study, both the OK and MOK models outperformed the MAR, SHAO, and RWEQ models. The RWEQ model, though based on physical processes that impact aeolian transport, is a largely empirical model, with the forms of equations and their constants unconstrained by the physics of aeolian transport. The form of Equations (30) and (31), for instance, do not seem to be determined by any physical process, even though λ and F_g certainly are related to the processes in question. Nonetheless, the RWEQ model has a significant advantage over the MAR and SHAO models, at least as far as the dataset used here is concerned; the RWEQ models predicted transport for all of our sites (Table 12). Unfortunately, the values it predicted showed little relation to those that were measured (ε_r = 240). In contrast, the MAR and SHAO models failed to predict transport for many of our sites (Table 12). Modifications to the parameterization of z_o by increasing the roughness 100-fold, to bring z_o into the same order of magnitude as for the OK and MOK models, results in predicted transport for 34 of the sites in the MAR model and 63 of the sites in the SHAO model, but r and ε_r (for the sites for which flux is predicted) for these scenarios are quite bad (MAR: r=0.02 ε_r=5600; SHAO: r=0.02 ε_r=2400). The failure to predict flux at many sites, particularly since the sites where transport was not modeled were not simply those locations with the lowest transport, suggests difficulties in their representation of the surface.

The OK (and MOK) models treat the surface fundamentally differently from the MAR and SHAO models. In the OK models, horizontal flux is possible in some locations of the landscape that are exposed while other, more protected areas do not experience transport. In the MAR and SHAO models, the entire landscape is characterized by a single threshold and transport must occur everywhere at the same time, or not at all. In other words, according to the OK models, vegetation alters the *distribution* of shear stress on the surface, whereas in the MAR and SHAO models, vegetation changes the threshold shear stress for the entire surface. Field observations [e.g., *Gillette et al.*, 2006] show that flux does not have to occur on the landscape at all places during a transport event. In this sense, the OK models represent the physics of transport better than the MAR and SHAO models. The fact that the OK models show better correspondence with our field data provides further support for this view of vegetation's impact on aeolian transport.

Aeolian transport is a threshold-controlled process and flux is nonlinear when shear velocity exceeds the threshold. Therefore, the difference between measured and modeled values of horizontal flux is highly dependent upon errors in wind speed and threshold shear velocity. To examine the impact of uncertainty in these site-level parameters, we examined the sensitivity of our error estimates on uncertainty in mean windspeed and u_{*t}. Other parameters also carry uncertainty, but these two have the largest impact on model error. Uncertainty in u_{*t} and mean wind speed of 5% using our simulation approach gave a minimum ε_r of 0.4, whereas uncertainty at the level of 25% for both of these site-level parameters gave a 1 ε_r of ~ 7 (Figure 6A). Our validated models using both *Gillette and Passi* [1988] and *Sorensen* [1991] gave ε_r of 2.1 (uncorrected). These uncorrected ε_r values are consistent with a total uncertainty of mean wind speed and u_{*t} of ~25% - 35% (Figure 6B). The method used in this study for estimation of u_{*t} is associated with an error of about 10% *[Li et al.*, 2010] and in this study, we were not able to measure u_{*t} during the period of flux measurement, meaning that the error in u_{*t} is likely greater than 10%. Furthermore, we were constrained to use a relatively small number of meteorological observation stations that were, in some cases, quite distant from the site where flux was estimated. Thus, wind speed measurements were not exactly collocated with flux estimates, likely resulting in considerable mismatch between the winds experienced by the site and the wind speed records used in the model calibration/validation. Given the uncertainty of these site-level parameters, it is highly unlikely that the model might have estimated flux with ε_r of less than 2 or 3. We therefore consider that uncertainty in wind speed and u_{*t} is contributing significantly to our model error and that ε_r ~ 2.1 constitutes a very good agreement between measured and modeled values.

5. Conclusions

In this study, we parameterized and validated the *Okin* [2008] wind erosion model on a variety of field sites ranging from shrubby grassland in southern New Mexico to grassland and shrubland in Utah and California, including both relatively degraded and undegraded plant communities. The model predicted the occurrence of wind erosion at each of the sites during the experimental period, which is in agreement with the field observations, with approximate relative errors of 2.1, which we consider satisfactory, particularly given constraints in knowledge of wind speed and u_{*t}. Empirical corrections were able to further improve approximate relative error, bringing it to 1.0. The OK model also predicted flux better than a revised version and three other published models. This comparison is made both on the basis of the statistics for those sites where transport was modeled (i.e., r and ε_r) and the number of sites on which it was modeled.

In the OK model, the distribution of shear stress on the surface is modified by the presence and distribution of vegetation. In the MAR and SHAO models, vegetation alters shear stress on the surface, but this effect is only incorporated into the model as the average change in shear stress. This difference allows the OK model to predict flux at higher vegetation covers than the MAR and SHAO models. The effect of changing the distribution of shear stress on the surface rather than merely changing the average shear stress experienced by the surface is seen in the inability of the MAR and SHAO models to predict transport for many of our sites.

No modeling study can, by itself, show that one physical model is better than another, especially in systems as complex as those investigated here. Nonetheless, our results suggest that the understanding of vegetation's impact of shear stress in the OK model is a more realistic representation of the physics involved in aeolian transport. Of course, some aspects of our understanding of transport in real environments remain elusive. Our results indicate clearly that the u_{*t} that leads to sediments captured in aeolian traps is in effect lower than that estimated directly, even over a relatively large area in the vicinity of the trap. This result suggests that temporal and spatial variability of u_{*t} in vegetated landscapes is likely a fruitful avenue of research for the future. In addition, the positive correlations of plant height, vegetation cover, and u_{*t} with model error suggest directions for the modification of the model. In particular, we believe that modification of the model to incorporate capture of saltating material by vegetation would improve it. There has been some theoretical work on this [e.g., *Raupach et al.*, 2001] and some work in well-controlled outdoor systems [*Gillies et al.*2006], but so far as we know, no field research in natural landscapes.

A further advantage of the OK model over the alternate models is the ease with which vegetation parameters can be measured. Despite its long history, λ is extremely difficult to measure in the field. Gap size distribution, in contrast may be obtained by a standard transect-based vegetation survey technique [e.g., *Herrick et al.*, 2005]. Recent research by *Vest et al.*

[2012] supports this view. Alternatively, vegetation characteristics could be obtained by an image-based technique [*Karl et al.*, 2011 ; *McGlynn and Okin*, 2006], supplemented by knowledge of plant height. Additionally, the recent development of high resolution terrestrial laser scanner [e.g., *Jupp et al.*, 2008] or airborne lidar might make it possible to capture the distribution of unvegetated gaps and canopy height at a much higher spatial resolution, minimizing the possibility of missing wind erosion "hot spots" while using the line-intercept method.

Development of the OK model was motivated by observations of aeolian processes in semiarid shrubby grasslands of the southwestern United States and it was subsequently developed for estimating wind erosion in rangeland ecosystems. However, because the model is based on shear velocity partitioning and physical principles, its use may not be limited to rangelands. Further investigation is required to implement the OK model in other ecosystems, particularly agricultural lands, where wind erosion models have existed for decades.

This study shows that the OK model provides superior flux estimates in vegetated systems. With the calibration and error analysis that was conducted here, it is now suitable for use in modeling transport in the world's drylands. In the US, the Natural Resource Conservation Service's (NRCS's Natural Resource Inventory (NRI) program [*Toevs et al.*, 2011], which has data on over 10,000 points in non-federal lands in the Western US, uses vegetation monitoring protocols that provide information on gap size and vegetation height and are, therefore, fully consistent with the OK model. NRI methods have also been recently adopted by the Bureau of Land Management for application to most federally owned rangelands in the United States. An electronic field data collection system is now available which automatically provides the gap and height information required [*Courtright and Van Zee*, 2011]. Similar data are now being collected as part of Mongolia's national monitoring system and used in a number of countries including China and Mexico. Compatible data can be collected by pastoralists using even simpler methods [*Riginos et al.*, 2011]. As consistent gapsize datasets are developed for other lands, the OK model could provide improved modeling of aeolian transport elsewhere. Moving beyond local or regional studies, incorporating the OK model into global models of aeolian transport may improve estimates in vegetated regions, thus improving underestimations in these regions and contributing to better modeling of changing dust emission in response to global environmental change. This step will require reliable ways to translate modeled or remotely-sensed estimates of vegetation cover into gap size.

Acknowledgements

We thank Matthew Van-Scoyoc and Michelle Mattocks for their assistance in collecting soil and vegetation data. We also acknowledge Frank Urban for providing wind data for some of the Utah sites. This research was supported by the USDA-Agricultural Research Service, the USDA-Natural Resources Conservation Service Conservation Effects Assessment Program, the U.S. Geological Survey, the Bureau of Land Management, and NSF EAR Grants 0720218 and NASA Grant NNX10AO97G. Any use of trade names is for descriptive purposes only and does not imply endorsement by the U.S. Government.

References

Belnap, J., R. L. Reynolds, M. C. Reheis, S. L. Phillips, F. E. Urban, and H. L. Goldstein (2009), Sediment losses and gains across a gradient of livestock grazing and plant invasion in a cool, semi-arid grassland, colorado plateau, USA, *Aeolian Res.*, 1:27-43, doi:10.1016/j.aeolia.2009.03.001.

Bergametti, G., and D. A. Gillette (2010), Aeolian sediment fluxes measured over various plant/soil complexes in the chihuahuan desert, *J. Geophys. Res.*, 115, F03044, doi:10.1029/2009JF001543.

Bradley, E. F., and P. J. Mulhearn (1983), Development of velocity and shear-stress distributions in the wake of a porous shelter fence, *J. Wind Eng. Indust. Aerodyn.*, 15 (1-3): 145-156.

Buschiazzo, D. E., and T. M. Zobeck (2008), Validation of weq, rweq and weps wind erosion for different arable land management systems in the argentinean pampas, *Earth Surf. Proc. Land*. 33:1839-1850, doi: 10.1002/esp.1738.

Courtright, E., and J. W Van Zee (2011), The database for inventory, monitoring and assessment (DIMA), *Rangelands*, 33(4):21-26, doi: http://dx.doi.org/10.2111/1551-501X-33.4.21.

Feng, G., and B. Sharratt (2007), Validation of WEPS for soil and PM10 loss from agricultural fields within the Columbia Plateau of the United States, *Earth Surf. Proc. Land*., 32, 743-753, doi: 10.1002/esp. i434.

Feng, G., and B. Sharratt (2009), Evaluation of the SWEEP model during high wind on the Columbia Plateau, *Earth Surf. Proc. Land.*, 34, 1461-1468, doi, 10.1002/esp.1818.

Fryrear, D. W. (1986), A field dust sampler, *J. Soil Water Conserv*., 41: 117-120.

Fryrear, D. W., A. Saleh, J. D. Bilbro, H. M. Shomberg, J. E. Stout, and T. M. Zobeck (1998), Revised Wind Erosion Equation*Rep.*, USDA ARS, Wind Erosion and Water Conservation Research Unit, Manhattan, Kansas.

Gillette, D. A. (1977), Fine particulate emissions due to wind erosion, Trans. Am. Soc. Agric. Eng., *20*(5), 890-897.

Gillette, D. A., and R. Passi (1988), Modeling of dust emission caused by wind erosion, *J. Geophys. Res.*, 93: 14,223-14,242.

Gillette, D. A., and W. A. Chen (2001), Particle production and aeolian transport from a "supply limited" source area in the Chihuahuan Desert, New Mexico, United States, *J. Geophys. Res.*, 106: 5267-5278.

Gillette, D. A., J. E. Herrick, and G. A. Herbert (2006), Wind characteristics of mesquite streets in the Northern Chihuahuan Desert, New Mexico, USA, *Environ. Fluid Mech.*, 6: 21-275, doi 10.1007/s10652-005-6022-7.

Gillies, J. A., W. G. Nickling, and J. King (2006), Aeolian sediment transport through large patches of roughness in the atmospheric inertial sublayer, *J. Geophys. Res.*, 111, F02006, doi: 10.1029/2005JF000434.

Griffin, D. W., V. H. Garrison, J. R. Herman, and E. A. Shinn (2001), African desert dust in the Caribbean atmosphere: Microbiology and public health, *Aerobiologia*, 17: 203-213.

Herrick, J. E., J. W. Van Zee, K. M. Havstad, L. M. Burkett, and W. G. Whitford (2005), *Monitoring manual for grassland, shrubland and savanna ecosystems*, vol 1: quick start, Tucson, AZ, University of Arizona Press.

Jupp, D. L. B., D. S. Culvenor, J. L. Lovell, G. J. Newnham, A. H. Strahler, and C. E. Woodcock (2008), Estimating forest LAI profiles and structural parameters using a ground-based laser called 'Echidna', *Tree Physiol*., 29: 171-181. doi: 10.1093/treephys/tpn022.

Karl, J. W., M. C. Duniway, and T. S. Schrader (2011), A Technique for Estimating Rangeland Canopy-Gap Size Distributions From High-Resolution Digital Imagery, *Rangeland Ecol. Manag. 65*(2), 196-207, doi: http://dx.doi.org/10.2111/REM-D-11-00006.1.

Kawamura, R. (1951), Study of sand movement by wind, *Hydraulic Engineering Laboratory Report HEL-2-8*, pp 57, Univ. of California, Berkeley, Calif.

King, J., W. G. Nickling, and J. A. Gillies (2005), Representation of vegetation and other nonerodible elements in aeolian shear stress partitioning models for predicting transport threshold, J. Geophys. Res., 110, F04015, doi:10.1029/2004JF000281.

Lancaster, N., and A. Baas (1998), Influence of vegetation cover on sand transport by wind: Field studies at Owens Lake, California, *Earth Surf. Proc. Land*. 23: 69-82.

Lettau, K., and H. H. Lettau (1978), Experimental and micro-meteorological field studies of dune migration. In: *Exploring the World's Driest Climate*, edited by H. H. Lettau and K. Lettau, IES Report, 101, pp. 110-147, Univ. of Wisconsin-Madison, Institute for Environmental Studies, Madison, Wisc.

Li, J., G. S. Okin, L. Alvarez, and H. Epstein (2007), Quantitative effects of vegetation cover on wind erosion and soil nutrient loss in a desert grassland of southern New Mexico, USA, *Biogeochemistry*, 85: 317-332, doi: 10.1007/s10533-007-9142-y.

Li, J., G. S. Okin, L. Alvarez, and H. Epstein (2008), Effects of wind erosion on the spatial heterogeneity of soil nutrients in two desert grassland communities, *Biogeochemistry*, 88: 73-88, doi: 10.1007/s10533-008-9195-6.

Li, J., G. S. Okin, J. E. Herrick, J. Belnap, S. M. Munson, and M. E. Miller (2010), A Simple Method to Estimate Threshold Friction Velocity of Wind Erosion in the Field, *Geophys. Res. Lett.*, *37*, L10402, doi:10.1029/2010GL043245.

Mahowald, N. M., C. S. Zender, C. Luo, D. Savoie, O. Torres, and J. del Carral (2002), Understanding the 30-year Barbados desert dust record, *J. Geophys. Res.*, 107D(21), 4561, doi: 10.1029/2002JD002097.

Marshall, J. K. (1971), Drag measurements in roughness arrays of varying density and distribution, *Agr. Meteorol.*., 8: 269-292.

Marticorena, B., and G. Bergametti (1995), Modeling the atmospheric dust cycle: 1. Design of a soil-derived dust emission scheme, *J. Geophys. Res.*, 100, 16,415-16,430.

Marticorena, B., G. Bergametti, D. Gillette, and J. Belnap (1997a), Factors controlling threshold friction velocity in semiarid and arid areas of the United States, *J. Geophys. Res.*, 102: 23,277-23,287.

Marticorena, B., G. Bergametti, B. Aumont, Y. Callot, and M. Legrand (1997b), Modeling the atmospheric dust cycle: 2. Simulation of Saharan sources, *J. Geophys. Res.*, 102: 4387-4404.

McGlynn, I. O., and G. S. Okin (2006), Characterization of shrub distribution using high spatial resolution remote sensing: ecosystem implication for a former Chihuahuan Desert Grassland, *Remote Sens. Environ*., 101(4): 554-566, doi: 10.1016/j.rse.2006.01.016.

Minvielle, F., B. Marticorena, D. A. Gillette, R. E. Lawson, R. Thompson, and G. Bergametti (2003), Relationship between the aerodynamic roughness length and the roughness density in cases of low roughness density, *Environ. Fluid Mech*., 3(3), 249– 267.

Okin, G. S. (2008), A new model of wind erosion in the presence of vegetation, *J. Geophys. Res.*, 113: F02S10, doi: 10.1029/2007JF000758.

Okin, G. S., and D. A. Gillette (2001), Distribution of vegetation in wind-dominated landscapes: Implications for wind erosion modeling and landscape processes, *J. Geophys. Res.*, 106: 9673-9683.

Owen, P. R. (1964), Saltation of uniform sand grains in air, *J. Fluid Mech.*, 20: 225-242.

Painter, T. H., A. P. Barrett, C. C. Landry, J. C. Neff, M. P. Cassidy, C. R. Lawrence, K. E. McBride, and G. L. Farmer (2007), Impact of disturbed desert soils on duration of mountain snow cover, *Geophys. Res. Lett.*, 34: L12502, doi: 10.1029/2007GL030284.

Painter, T. H., J. Deems, J. Belnap, A. Hamlet, C. C. Landry, and B. Udall (2010), Response of Colorado River runoff to dust radiative forcing in snow, *Proc. Natl. Acad. Sci*. USA, vol. 107 (40):17,125-17,130, doi: 10.1073/pnas.0913139107.

Raupach, M. R, D. A. Gillette, and J. F. Leys (1993), The effect of roughness elements on wind erosion threshold, *J. Geophys. Res.*, 98: 3023-3029.

Raupach, M. R. (1992), Drag and drag partition on rough surfaces, *Bound-Lay Meteorol.*, *60*, 375-395.

Raupach, M. R., N. Woods, G. Dorr, J. F. Leys, and H. A. Cleugh (2001), The entrapment of particles by windbreaks, *Atmos Environ*, *35*(20), 3373-3383.

Reynolds, J., and D. M. Stafford Smith (Eds.) (2002), *Global Desertification: Do Humans Cause Deserts?*, 437 pp., Dahlem University Press, Berlin.

Reynolds, R., J. Belnap, M. Reheis, P. Lamothe, and F. Luiszer (2001), Aeolian dust in Colorado Plateau soils: Nutrient inputs and recent change in source, *Proc. Natl. Acad. Sci*. USA, vol. 98 (13): 7123-7127, doi: 10.1073/pnas.121094298.

Riginos, C., J. E. Herrick, S. R. Sundaresan, C. Farley, and J. Belnap (2011), A simple graphical approach to quantitative monitoring of rangelands, *Rangelands*, 33(4): 6-13, doi: http://dx.doi.org/10.2111/1551-501X-33.4.6.

Rohlf, F. J. and R. R. Sokal (1981), *Statistical tables, 2 edition*. W.H. Freeman and Company, New York.

Seager, R., M. Ting, I. Held, Y. Kushnir, J. Lu, G. Vecchi, H. Huang, N. Harnik, A. Leetmas, N. Lau, C. Li, J. Velez, and N. Naik (2007), Model projections of an imminent transition to a more arid climate in southwestern North America, *Science*, 316: 1181-1184, doi: 10.1126/science.1139601.

Shao, Y. (2008), *Physicis and Modeling of Wind Erosion*, 2ed., Springer, New York.

Shao, Y., and M. R. Raupach (1992), The overshoot and equilibration of saltation, *J. Geophys. Res.*, 97: 20,559-20,564.

Shao, Y., M. R. Raupach, and P. A. Findlater (1993), The effects of saltation bombardment on the entrainment of dust by wind, *J. Geophys. Res.*, 98: 12,719-12,726.

Sokolik, I. N., and O. B. Toon (1996), Direct radiative forcing by anthropogenic airborne mineral aerosols, *Nature*, 381: 681-683.

Sorensen, M. (1991), An analytical model of windblown sand transport, In: *Aeolian Grain Transport: Mechanics*, edited by O. E. Barndorff-Nielsen and B. B. Willetts, Acta Mechanica Supplement 1: 67-81.

Tegen, I., S. P. Harrison, K. Kohfeld, I. C. Prentice, M. Coe, and M. Heimann (2002), Impact of vegetation and preferential source areas on global dust aerosol: Results from a model study, *J. Geophys. Res.*, 107, 4576, doi:10.1029/2001JD000963.

Thomas, D. S. G., M. Knight, and G. F. S. Wiggs (2005), Remobilization of southern African desert dune systems by twenty-first century global warming, *Nature*, *435*(7046), 1218-1221, doi:10.1038/nature03717.

Toevs, G. R., J. W. Karl, J. J. Taylor, C. S. Spurrier, M. Karl, M. R. Bobo, and J. E. Herrick (2011), Consistent indicators and methods and a scalable sampling design to meet assessment, inventory, and monitoring information needs across scales, *Rangelands*, 33(4): 14-20, doi: http://dx.doi.org/10.2111/1551-501X-33.4.14.

Van Pelt, R. S., T. M. Zobeck, K. N. Potter, J. E. Stout, and T. W. Popham (2004), Validation of the wind erosion stochastic simulator (wess) and the revised wind erosion equation (rweq) for single events, *Environ. Modell. Softw*., 19:191-198.

Vest, K., A. J. Elmore, J. M. Kaste, G. S. Okin, and J. Li (2012), Estimating total horizontal aeolian flux within shrub-invaded groundwater dependent meadows using empirical and mechanistic models, *J. Geophys. Res.*, *Revision submitted.*

Zender, C. S., H. Bian, and D. Newman (2003), The mineral dust entrainment and deposition (DEAD) model: Description and 1990s dust climatology, *J. Geophys. Res.*, 108 (D4): 4416, doi: 10.1029/2002JD002775.

Figure captions

Figure 1. Horizontal flux vs. Lateral cover for field experiments *(a, b)* and model prediction *(c)*. *(a)* data from individual storms from Owens Dry Lake [*Lancaster and Baas*, 1998], *(b)* data from two seasons in the Chihuahuan Desert [*Li et al.*, 2007], and *(c)* estimates of total horizontal flux using the shear-stress partitioning model of *Raupach et al.* [1993] and the flux equation of *Shao and Raupach* [1992] using two values of *m*, 0.5 and 1.0. Light lines are horizontal flux estimated

at constant shear velocity (1.0 m s^{-1}) and heavy lines are flux estimates for actual wind speed records of the Jornada Experimental Range in New Mexico from 1997 to 2001. Figure redrawn from *Okin* [2008].

Figure 2. An example of a histogram of the scaled gap size, constructed based on the size of a gap and the height of an adjacent plant canopy for all gaps and canopies along three 50-m transects at each site.

Figure 3. Relationship between z'_o and z_o given by Equation (12) and used for the determination of roughness length in the MOK model.

Figure 4. Frequency distribution of windspeeds used in the mass flux modeling for major study sites. More details related to the characteristics of the study sites may be found in Tables 1 and S1.

Figure 5. Horizontal mass flux (Q_t, act, g m-1 d-1) measured by BSNEs located in the major study sites. More details of the study sites are listed in Table 1.

Figure 6. Expected error, plotted as ε_r, when u_{*t} and mean wind speed are uncertain. The degree of uncertainty is estimated using the coefficient of variation (CV). A) the surface plots ε_r against CV of mean wind speed and u_{*t}. The surface has been interpolated. B) ε_r plotted against the sum of the CVs of mean wind speed and u_{*t}.

Tables

Table 1. Locations and environmental characteristics of the study sites

	Moab, UT	Fivemile Mountain, UT	Clear Spot Flat, UT	Jornada Experimental Range, NM	Owens Valley, CA
Plant community	Shrubby grassland	Shrubland	Shrubland	Shrubby grassland	Shrubby grassland
Dominant species	*Sarcobatus vermiculatus, Atriplex canescens, Stipa comata*	*Artemisia tridentata*	*Atriplex confertifolia, Halogeton glomeratus, Salsola tragus*	*Prosopis glandulosa, Larrea tridentate, Bouteloua eriopoda*	*Sarcobatus vermiculatus, Atriplex torreyi, Distichlis spicata*
Treatment	-	Mechanically treated	Burned and Mechanically treated	Shrub removal[b]	-
Annual rainfall (mm)	230	340	227	247	128
Elevation (m)	1227	1515	1524	1250	1264
Soil texture	Sandy loam	Sandy loam-silt loam	Sandy loam, silt loam, loam	Sand	Loamy sand, sandy loam
Roughness elements	Vegetation, soil crust	Woody debris, vegetation	Vegetation, woody debris	Vegetation	Vegetation, rocks
Wind data	CLIM-MET[a]	On-site	On-site	On-site	On-site, WRCC[c]
Number of BSNEs	25	10	2	15	13
Duration of BSNE deployment	Mar-Jul 2009	Mar-Jul 2009	Mar-Jun 2009	Mar-Jun 2009	May-Sept 2009

[a] CLIM-MET-Southwest Climate Impact Meteorological Stations, operated by the U.S. Geological Survey Geology and Environmental Change Science Center.
[b] Shrub removal was conducted in part of the Jornada sites, see details in *Li et al.* [2007].
[c]WRCC-Western Regional Climate Center, operated by the Desert Research Institute.

Table 2. The characteristics of vegetation, wind, and estimated threshold shear velocity for unvegetated soils for the primary experimental sites

Parameters	Moab, UT	Fivemile Mountain, UT	Clear Spot Flat, UT	Jornada Experimental Range, NM	Owens Valley, CA
Fractional plant cover (%)	~0-58	9-33	~0-36	11-27	29-78
Max gap (m)	>50	8.0	47	21	34
Average gap (m)	3.07	0.82	11	2.52	1.62
Max gap/canopy height	2212	446	2292	994	752
Average gap/canopy height	66	18	282	48	20
Max wind speed (m s^{-1})	12.0[a]	13.9[a]	15.2[a]	18.3[b]	26.4[b]
Threshold shear velocity (u_{*t}, m s^{-1})	0.26-0.97	0.31-0.54	0.26-1.04	0.19-0.54	0.36-0.91

[a] at the height of 3 m, [b] at the height of 10 m

Table 3. Description of the important input parameters used in the model

Parameters	Physical meaning	Range/value in literature	Relevant literature
z_o	Roughness length, m	10^{-7}- 10^{-1} m	*Marticorena et al.* [1997a]; *Gillette et al.*[2006]
A	Dimensionless constant	0 - 1	*Gillette et al.* [2001]
C	*e*-folding distance for recovery of the shear stress in the lee of plants, dimensionless	4.8 - 10	*Minvielle et al.* [2003], *Okin* [2008]
$\left(\frac{u_{*s}}{u_*}\right)_{x=0}$	Shear velocity ratio in the immediate lee of a plant, dimensionless	0.0 – 0.32	*Okin* [2008], *Bradley and Mulhearn* [1983]

Table 4. Representative mass flux equations used in the total horizontal mass flux calculation

	Expression	Citation
$Q_{t,\,pred} \propto u_*^{\,4}$	$A\dfrac{\rho}{g}u_*^4\left(1-\dfrac{u_{*t}}{u_*}\right)$	*Gillette and Passi* [1988]
$Q_{t,\,pred} \propto u_*^{\,3}$	$A\dfrac{\rho}{g}u_*^3\left(1-\dfrac{u_{*t}^2}{u_*^2}\right)$	*Owen* [1964], *Shao et al.* [1993], and *Gillette et al.* [2001]
	$A\dfrac{\rho}{g}u_*^3\left(1-\dfrac{u_{*t}^2}{u_*^2}\right)\left(1+\dfrac{u_{*t}}{u_*}\right)$	*Kawamura* [1951]
	$A\dfrac{\rho}{g}u_*^3\left(1-\dfrac{u_{*t}}{u_*}\right)\left(1+17.75\,\dfrac{u_{*t}}{u_*}\right)$	*Sorensen* [1991]
	$A\dfrac{\rho}{g}u_*^3\left(1-\dfrac{u_{*t}}{u_*}\right)$	*Lettau and Lettau* [1978]
$Q_{t,\,pred} \propto u_*^{\,2}$	$A\dfrac{\rho}{g}u_*^2\left(1-\dfrac{u_{*t}^2}{u_*^2}\right)$	Modified *Shao et al.* [1993][*]

Note that the constants at the beginning of each of the original equations were replaced by a variable A that may be determined by model runs.

[*]The Shao *et al.* [1993] equation was revised to provide a relationship such that q scales with the second power of u_*.

Table 5. Bounding values of uniform distributions used for random selection of values for error minimization

Parameter	Minimum Value	Maximum Value
Log[A]	-6	-3
C	4.8	9.0
$\left(\frac{u_{*s}}{u_*}\right)_{x=0}$	0.0	0.4
Log[z_o]	-1.0	0.5

Table 6. Optimum mean values of OK model parameters obtained by leave-one-out cross-validation for different mass flux equations.

Mass flux equation (units)	z_o (m)	A (×10^{-3}) (g m^{-1} d^{-1})	C	$\left(\frac{u_{*S}}{u_*}\right)_{x=0}$
Gillette and Passi [1988]	0.077 ± 0.015	0.54 ± 0.23	5.6 ± 0.63	0.32 ± 0.072
Shao et al. [1993]	0.079 ± 0.015	26 ± 10	5.6 ± 0.89	0.29 ± 0.078
Kawamura [1951]	0.077 ± 0.015	16 ± 5.9	5.7 ± 0.75	0.31 ± 0.072
Sorensen [1991]	0.078 ± 0.015	7.3 ± 1.2	5.8 ± 0.86	0.31 ± 0.086
Lettau and Lettau [1978]	0.081 ± 0.015	39 ± 17	5.8 ± 0.93	0.30 ± 0.080
Modified *Shao et al.* [1993]	0.083 ± 0.012	780 ± 150	6.2 ± 1.0	0.28 ± 0.11

Table 7. Regression analysis of OK model performance in predicting total horizontal mass flux based on different mass flux equations

Mass flux equation	Slope[a]	Intercept[a,b]	r	ε_r
Gillette and Passi [1988]	1.06	0.069	0.67	2.1
Shao et al. [1993]	1.03	0.019	0.64	2.3
Kawamura [1951]	1.07	0.061	0.66	2.3
Sorensen [1991]	1.05	0.058	0.67	2.1
Lettau and Lettau [1978]	1.07	0.032	0.65	2.4
Modified *Shao et al.* [1993]	1.06	-0.57	0.64	6.0

[a] For regression of Log(predicted) vs. Log(actual), [b] units of Log[g m^{-1} d^{-1}]

Table 8. Stepwise regression analysis and the corrected errors by adding different factors for horizontal mass flux prediction. Calculations were based on the OK and the *Gillette and Passi* [1988] and *Sorensen* [1991] mass flux equations. Original r and ε_r refer to the cross-validation values in Table 7

Mass flux equation	Intercept	Plant height (m)	Fractional Cover, F_g	u_{*t} (m s^{-1})	Median windspeed (m s^{-1})	r	ε_r
Gillette	Original					0.67	2.1
and Passi	-0.41	0.024				0.73	1.4
[1988]	-0.49		1.61			0.60	1.6
	-0.59	0.020	0.88			0.70	1.2
	-1.21	0.022	0.68	0.014		0.72	1.1
	-1.97	0.020	1.15	0.015	0.0022	0.75	1.0
Sorensen	Original					0.67	2.1
[1991]	-0.42	0.025				0.57	2.1
	-0.48		1.60			0.59	1.7
	-0.59	0.021	0.82			0.70	1.3
	-1.24	0.023	0.62	0.14		0.72	1.0
	-1.78	0.021	0.95	0.15	0.0015	0.74	1.0

The empirically corrected horizontal mass flux values are given by original flux estimate + Intercept + Sum (Coefficient*Factor) for all of the factors.

Table 9. Optimum mean values of MOK model parameters obtained by leave-one-out cross-validation for different mass flux equations

Mass flux equation	A ($\times 10^{-3}$) (g m^{-1} d^{-1})	C	$(u_{*s}/u_*)_{x=0}$
Gillette and Passi [1988]	4.3 ± 0.72	5.1 ± 0.28	0.34 ± 0.045
Shao et al. [1993]	180 ± 27	5.1 ± 0.24	0.33 ± 0.063
Kawamura [1951]	110 ± 16	5.1 ± 0.24	0.33 ± 0.073
Sorensen [1991]	23 ± 3.3	5.1 ± 0.28	0.33 ± 0.059
Lettau and Lettau [1978]	310 ± 51	5.1 ± 0.23	0.33 ± 0.073
Modified *Shao et al.* [1993]	880 ± 72	5.3 ± 0.52	0.33 ± 0.071

Table 10. Regression analysis of MOK model performance in predicting total horizontal mass flux based on different mass flux equations.

Mass flux equation	Slope[a]	Intercept[a,b]	r	ε_r
Gillette and Passi [1988]	0.97	-0.052	0.56	3.0
Shao et al. [1993]	1.04	0.026	0.57	3.3
Kawamura [1951]	1.05	0.043	0.58	3.2
Sorensen [1991]	1.05	0.041	0.58	3.2
Lettau and Lettau [1978]	1.05	0.050	0.56	3.6
Modified *Shao et al.* [1993]	1.10	-1.29	0.56	33

[a] For regression of Log(predicted) vs. Log(actual), [b] units of Log[g m^{-1} d^{-1}]

Table 11. Stepwise regression analysis and the corrected errors by adding different factors for horizontal mass flux prediction. Calculations were based on the MOK and the *Gillette and Passi* [1988] mass flux equation. Original r and ε_r refer to the cross-validation values in Table 10.

Mass flux equation	Intercept	Plant height (m)	Fractional Cover, F_g	u_{*t} (m s^{-1})	Median windspeed (m s^{-1})	r	ε_r
Gillette and Passi [1988]	Original					0.56	3.0
	-0.28	0.018				0.57	2.6
	-1.32		0.028			0.54	2.1
	-1.73	0.020	0.030			0.57	1.6
	-1.72	0.021	0.030	-0.086		0.58	1.6
	-1.71	0.021	0.030	-0.090	-1.9×10^{-5}	0.58	1.6

The empirically corrected horizontal mass flux values are given by original flux estimate + Intercept + Sum (Coefficient*Factor) for all of the factors.

Table 12. Comparison of number of sites for which flux is predicted (n), Pearson correlation coefficient between $Q_{t,pred}$ and $Q_{t,act}$ (r), and relative prediction error (ε_r) models considered in this paper. The OK and MOK models used the *Gillette and Passi* [1988] flux equation and the values of the best-fit parameter values from Tables 6 and 9, respectively. Values for r and ε_r differ slightly from Tables 7 and 8 (for the OK model) and Tables 10 and 11 (for the MOK) model because they are not derived from cross-validation.

Model	n	r	ε_r
OK	65	0.68	2.0
MOK	65	0.59	2.8
MAR	3	0.52	0.6
SHAO	38	0.28	41
RWEQ	65	0.17	240

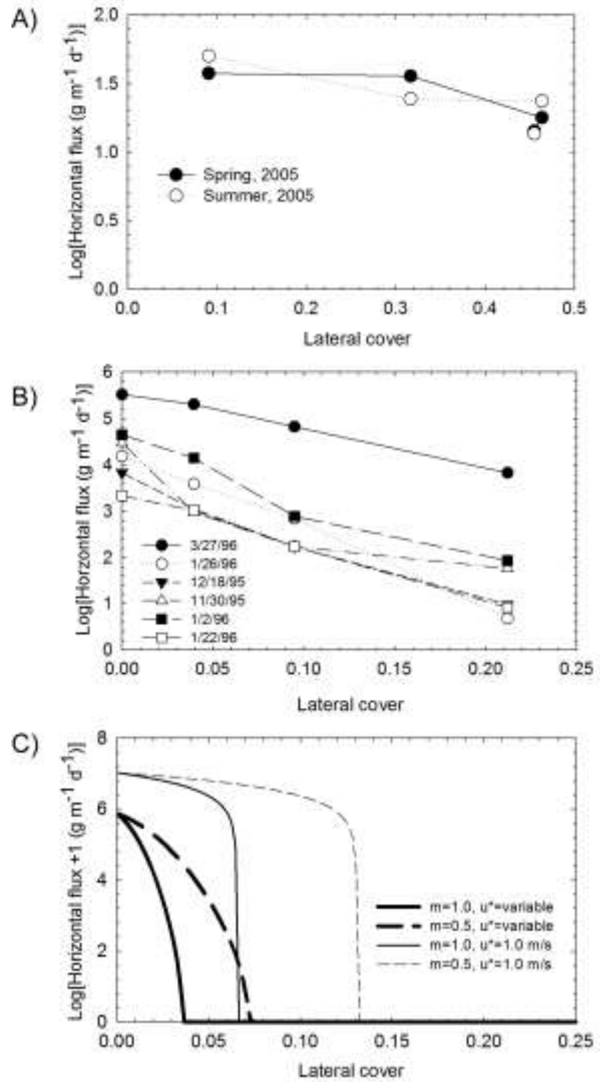

Figure 1. Horizontal flux vs. Lateral cover for field experiments *(a, b)* and model prediction *(c)*. *(a)* data from individual storms from Owens Dry Lake [*Lancaster and Baas*, 1998], *(b)* data from two seasons in the Chihuahuan Desert [*Li et al.*, 2007], and *(c)* estimates of total horizontal flux using the shear-stress partitioning model of *Raupach et al.* [1993] and the flux equation of *Shao and Raupach* [1992] using two values of *m*, 0.5 and 1.0. Light lines are horizontal flux estimated at constant shear velocity (1.0 m s^{-1}) and heavy lines are flux estimates for actual wind speed records of the Jornada Experimental Range in New Mexico from 1997 to 2001. Figure redrawn from *Okin* [2008].

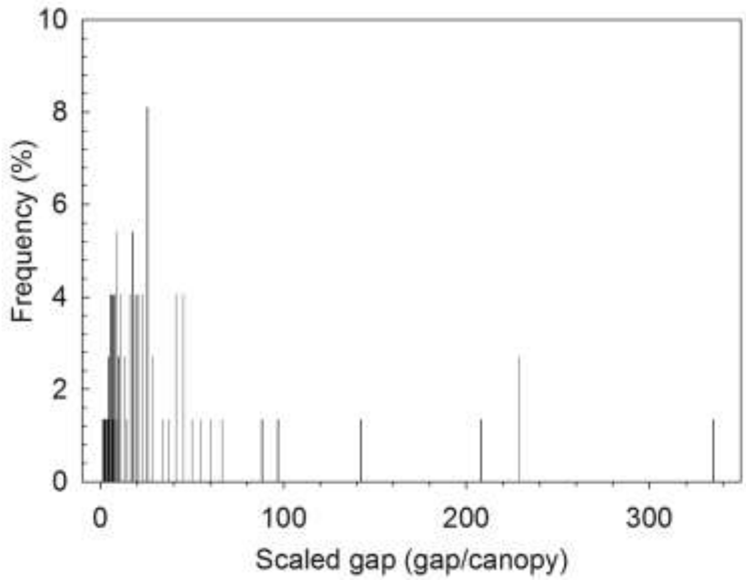

Figure 2. An example of a histogram of the scaled gap size, constructed based on the size of a gap and the height of an adjacent plant canopy for all gaps and canopies along three 50-m transects at each site.

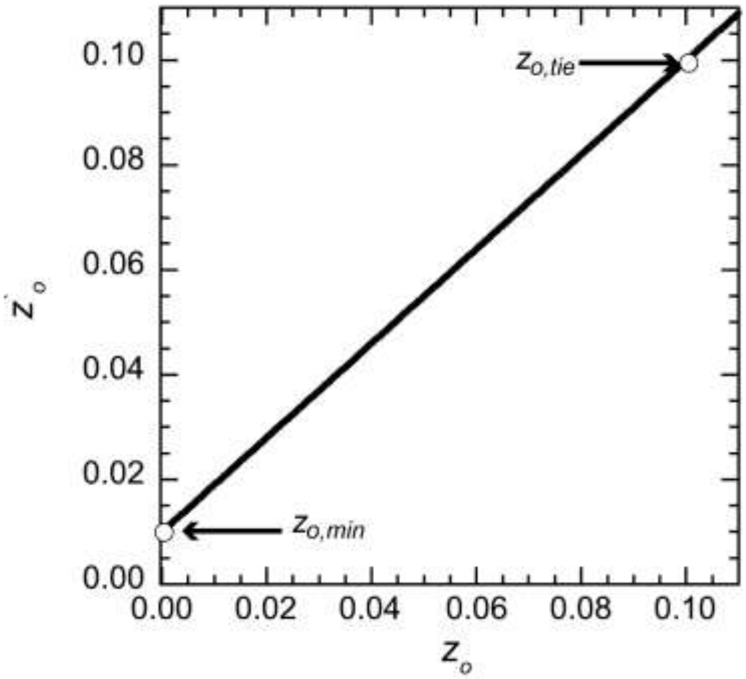

Figure 3. Relationship between z'_o and z_o given by Equation (12) and used for the determination of roughness length in the MOK model.

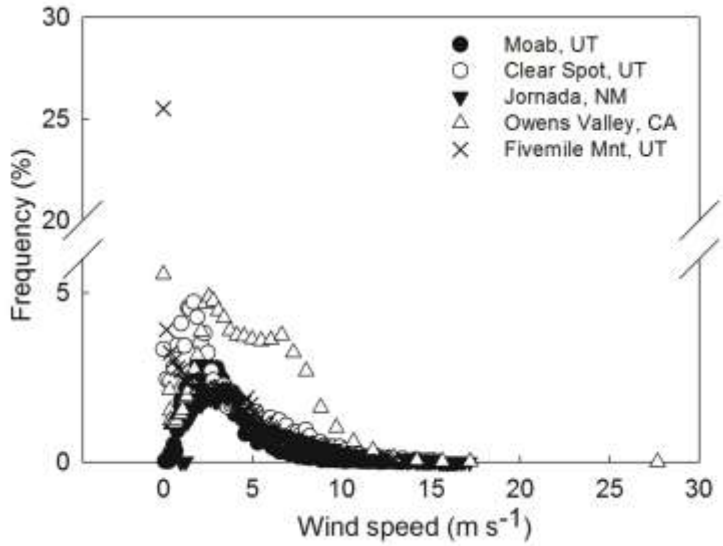

Figure 4. Frequency distribution of windspeeds used in the mass flux modeling for major study sites. More details related to the characteristics of the study sites may be found in Tables 1 and S1.

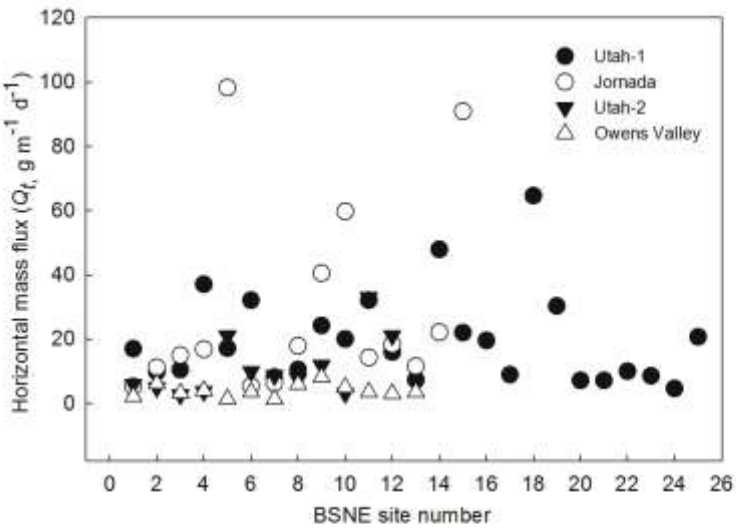

Figure 5. Horizontal mass flux (Q_t, act, g m-1 d-1) measured by BSNEs located in the major study sites. More details of the study sites are listed in Table 1.

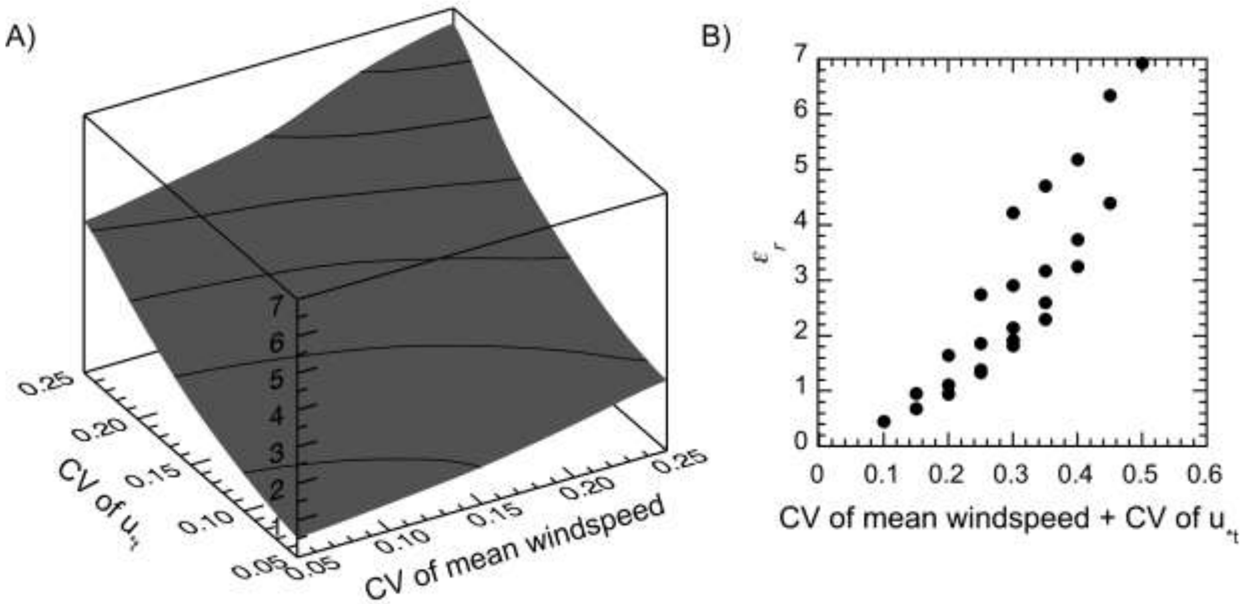

Figure 6. Expected error, plotted as ε_r, when u_{*t} and mean wind speed are uncertain. The degree of uncertainty is estimated using the coefficient of variation (CV). A) the surface plots ε_r against CV of mean wind speed and u_{*t}. The surface has been interpolated. B) ε_r plotted against the sum of the CVs of mean wind speed and $u_{*t.}$

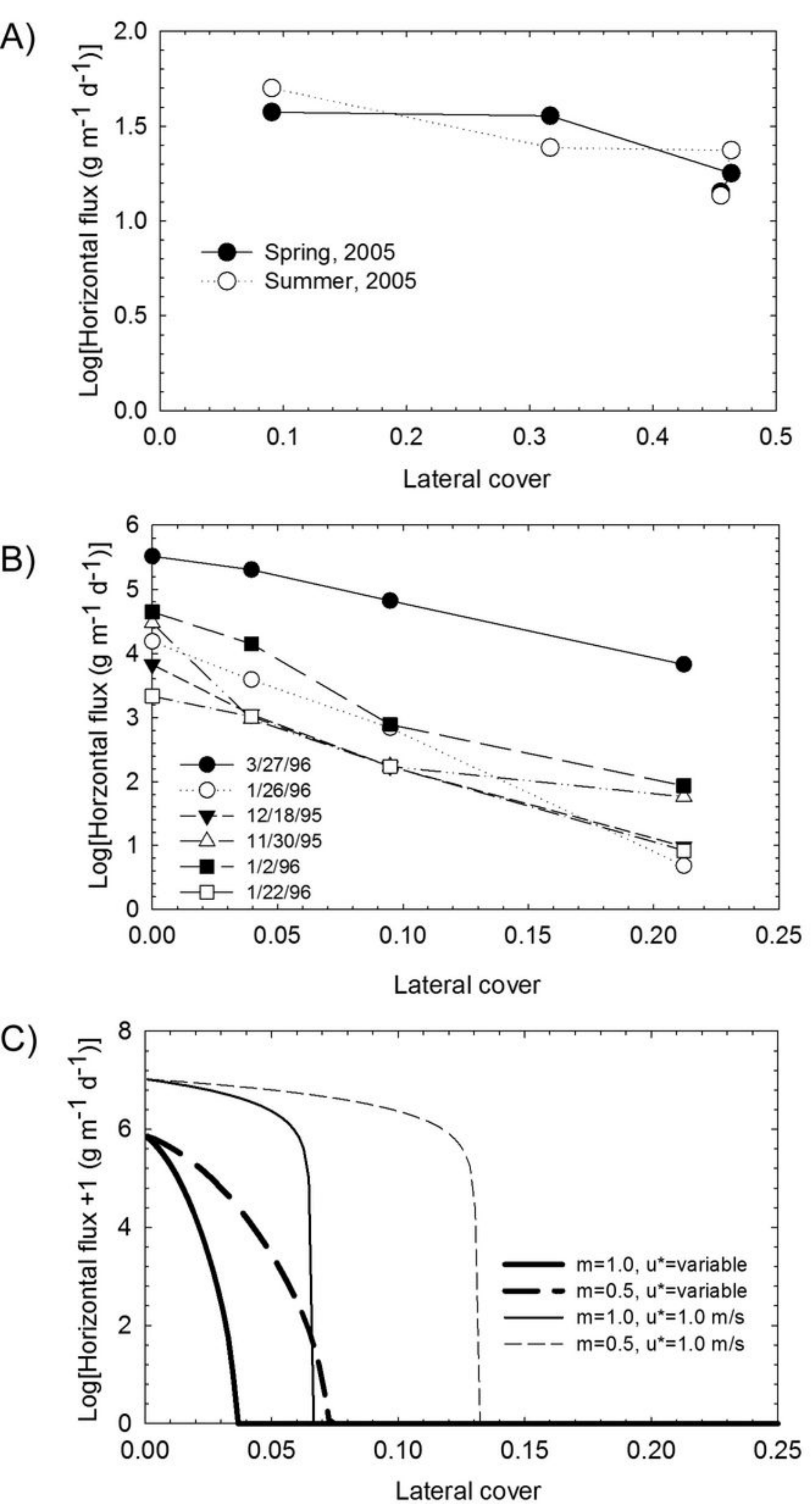
A)
Log[Horizontal flux (g m-1 d-1)]
2.0
1.5
1.0
0.5
0.0
0.1
0.2
0.3
0.4
0.5
Lateral cover
Spring, 2005
Summer, 2005
B)
Log[Horzontal flux (g m-1 d-1)]
6
5
4
3
2
1
0
0.00
0.05
0.10
0.15
0.20
0.25
Lateral cover
3/27/96
1/26/96
12/18/95
11/30/95
1/2/96
1/22/96
C)
Log[Horizontal flux +1 (g m-1 d-1)]
8
6
4
2
0
0.00
0.05
0.10
0.15
0.20
0.25
Lateral cover
m=1.0, u*=variable
m=0.5, u*=variable
m=1.0, u*=1.0 m/s
m=0.5, u*=1.0 m/s

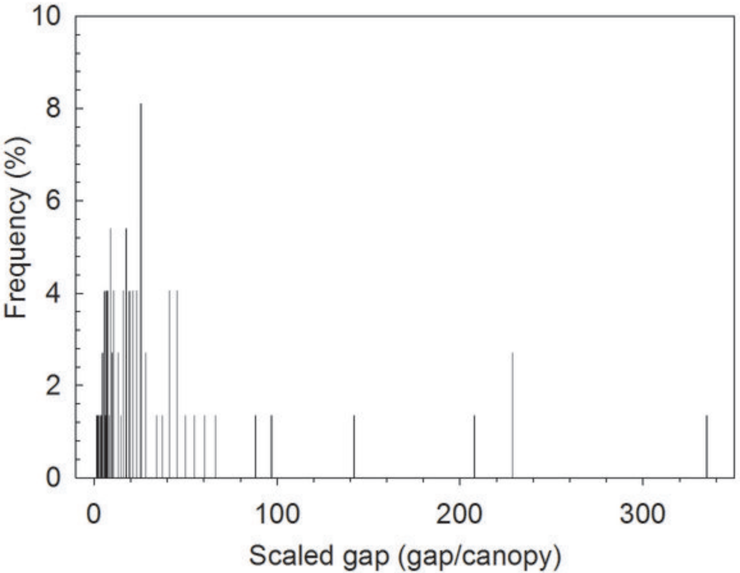
10
8
6
4
2
0
Frequency (%)
0
100
200
300
Scaled gap (gap/canopy)

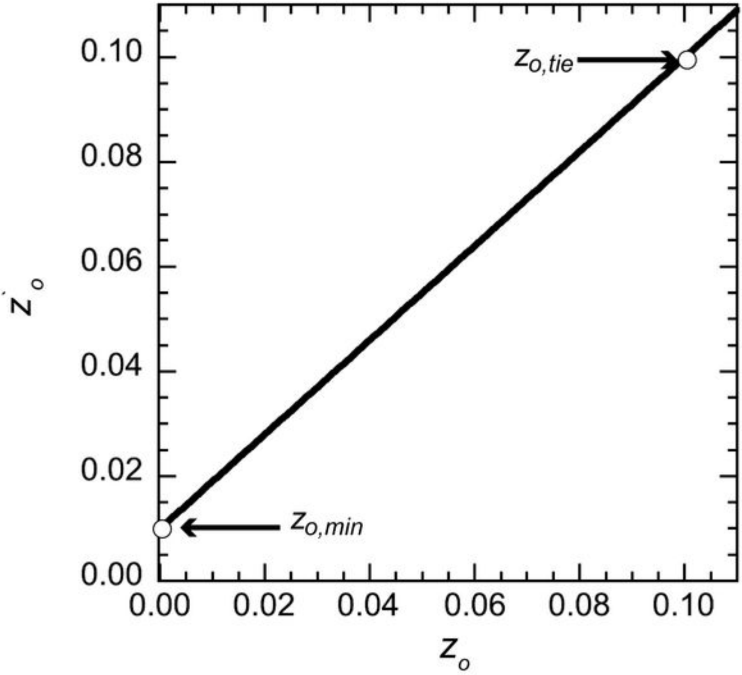

0.00
0.02
0.04
0.06
0.08
0.10
z_o'
z_o
$z_{o,tie}$
$z_{o,min}$

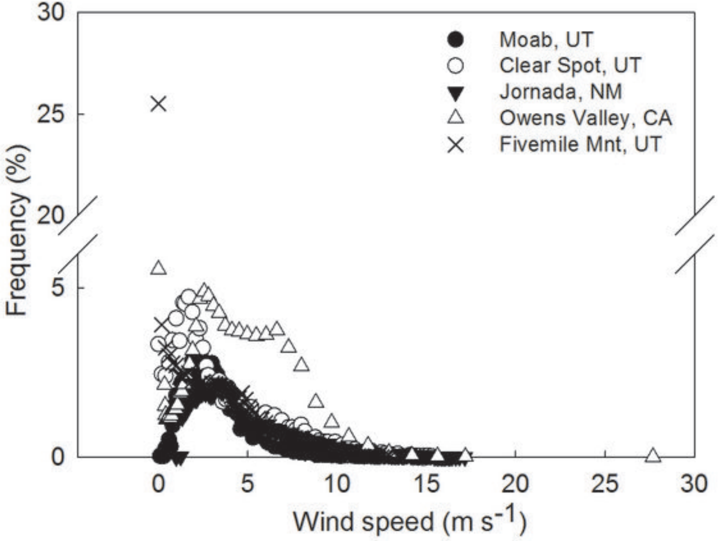

Moab, UT
Clear Spot, UT
Jornada, NM
Owens Valley, CA
Fivemile Mnt, UT
Frequency (%)
Wind speed (m s-1)
0
5
10
15
20
25
30
0
5
20
25
30

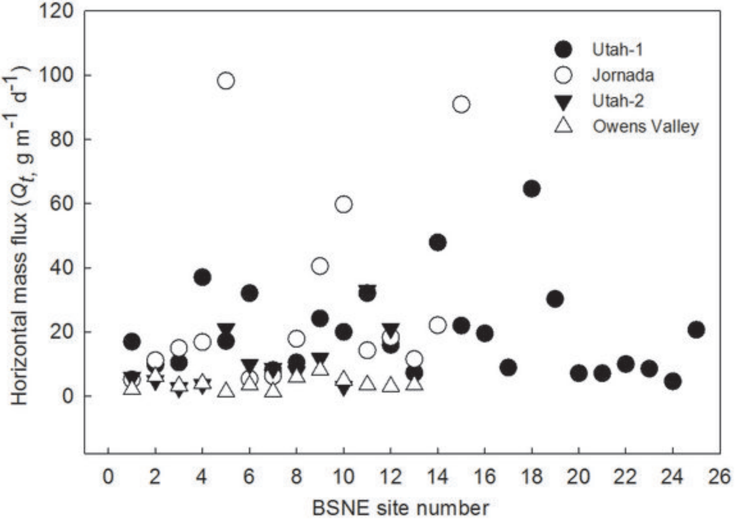

Utah-1
Jornada
Utah-2
Owens Valley
Horizontal mass flux (Q_t, g m^{-1} d^{-1})
BSNE site number
120
100
80
60
40
20
0
0
2
4
6
8
10
12
14
16
18
20
22
24
26

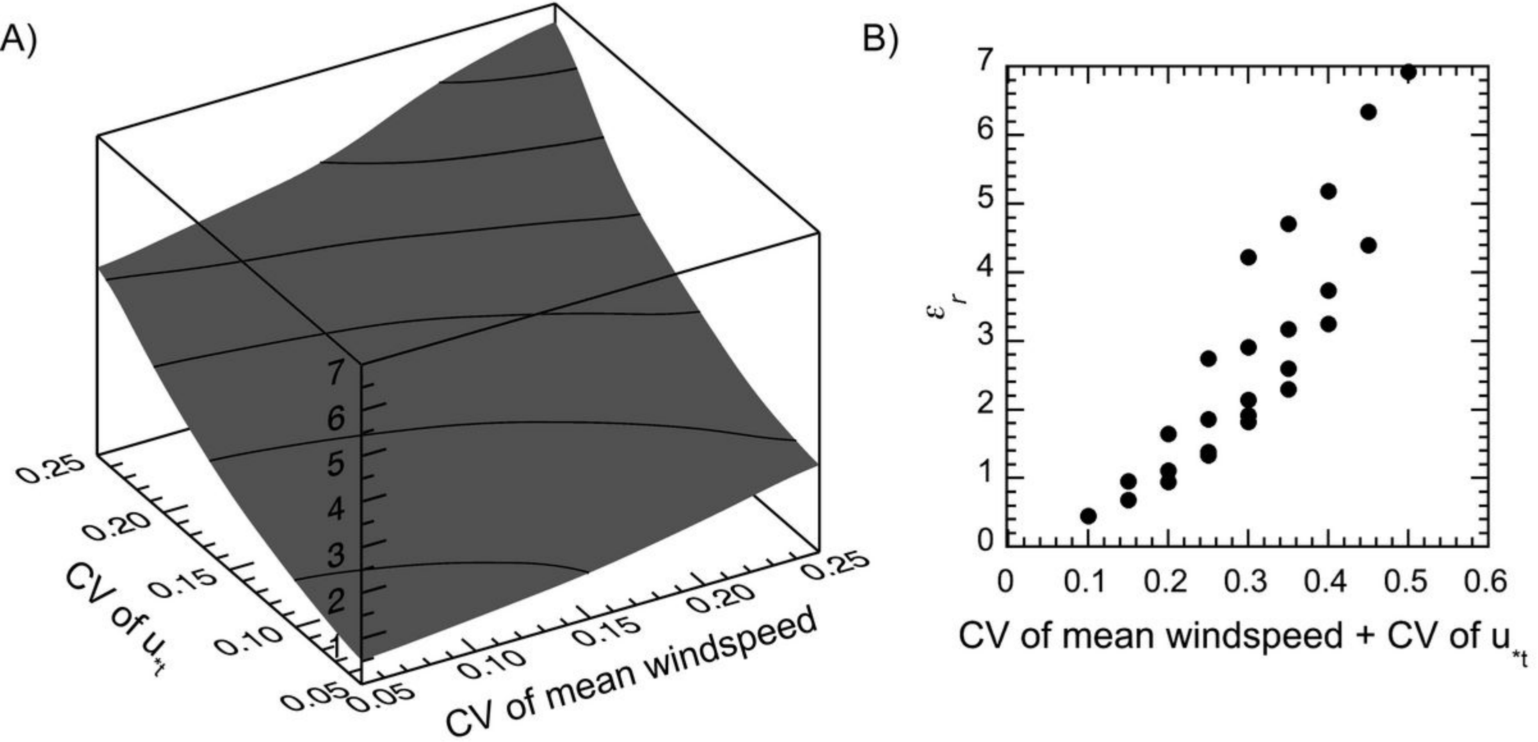
A)
B)
CV of u_{*t}
CV of mean windspeed
0.05
0.10
0.15
0.20
0.25
1
2
3
4
5
6
7
ε_r
0
0.1
0.2
0.3
0.4
0.5
0.6
CV of mean windspeed + CV of u_{*t}